NAIST-IS-DD1161028

Doctoral Dissertation

Rainfall Attenuation in Microwave Mesh Networks

Gemalyn Dacillo Abrajano

February 17, 2014

Department of Information Systems
Graduate School of Information Science
Nara Institute of Science and Technology

A Doctoral Dissertation
submitted to Graduate School of Information Science,
Nara Institute of Science and Technology
in partial fulfillment of the requirements for the degree of
Doctor of ENGINEERING

Gemalyn Dacillo Abrajano

Thesis Committee:

Professor Minoru OKADA	(Supervisor)
Professor Hiroyuki SEKI	(Co-supervisor)
Professor Keiichi YASUMOTO	(Co-supervisor)
Associate Professor Takeshi HIGASHINO	(Co-supervisor)

Rainfall Attenuation in Microwave Mesh Networks*

Gemalyn Dacillo Abrajano

Abstract

The propagation of microwave signals starting from 10 GHz in frequency is greatly affected by attenuation due to rainfall. The rainfall attenuation in a microwave link has been extensively studied in the past and attenuation models were used for the design and implementation of microwave links. Route diversity is used to lessen the effect of rain attenuation on the quality of communication networks. This study looks into the links' orientation and angular separation from each other in implementing the route diversity. Network configurations were simulated using real rainfall data to see the differences in attenuation for links oriented in different directions. The results showed significant gain for the route diversity. Another aim of this study is to determine the location and intensity of the rainfall field from the attenuation of a mesh network. Since microwave links are greatly attenuated by rainfall, this information on rainfall attenuation can be used to detect and reconstruct the rainfall field without using other weather sensors. However, its resolution is not enough for detecting the sporadic rain. This paper proposes an efficient use of compressed sensing algorithm for improving the resolution. The proposed method can identify intense rainfall rates like that of "guerilla rain", which are of interest because they can cause disasters. The proposed detection system can benefit areas that experience frequent heavy rains but do not have enough resources for weather sensing and forecasting.

Keywords:

Microwave mesh network, Rainfall attenuation, Compressed sensing, Sporadic heavy rain

*Doctoral Dissertation, Department of Information Systems, Graduate School of Information Science, Nara Institute of Science and Technology, NAIST-IS-DD1161028, February 17, 2014.

Contents

List of Figures

List of Tables

Chapter 1

Introduction

1 Research Motivation

In the most recent report of the Intergovernmental Panel on Climate Change (IPCC), climate scientists expressed renewed confidence on the effects of global warming and climate change in our environment [1]. In the extreme weather and climate events, the Working Group I to the Fifth Assessment Report said that it is "very likely" that there are now fewer cold days and nights while the warm days and nights have increased, and that it is "virtually certain" that the trend will continue even into the late 21st century. In fact, an article in *Nature* by scientists from the University of Hawaii reveals a new time frame for climate change [2]. Figure 1.1 shows the years when major cities in the world would start to have cool temperatures that are still warmer than what was experienced in the last 150 years. They are claiming that once this milestone is reached, there would be no going back to colder temperatures. This has a direct impact on both the sea level rise and extinction of many species. An irreversible increase in temperature will have the most impact in the tropical countries that are already generally hotter than the rest of the world.

The increase in atmospheric temperature also leads to the increase in ocean surface water temperature, which in turn leads to more tropical cyclones. Heavy precipitation events with increased frequency, intensity, and amount of heavy precipitation were also assessed to have increased since 1950, and will "very likely" increase more over most of the mid-latitude land masses and over wet tropical re-

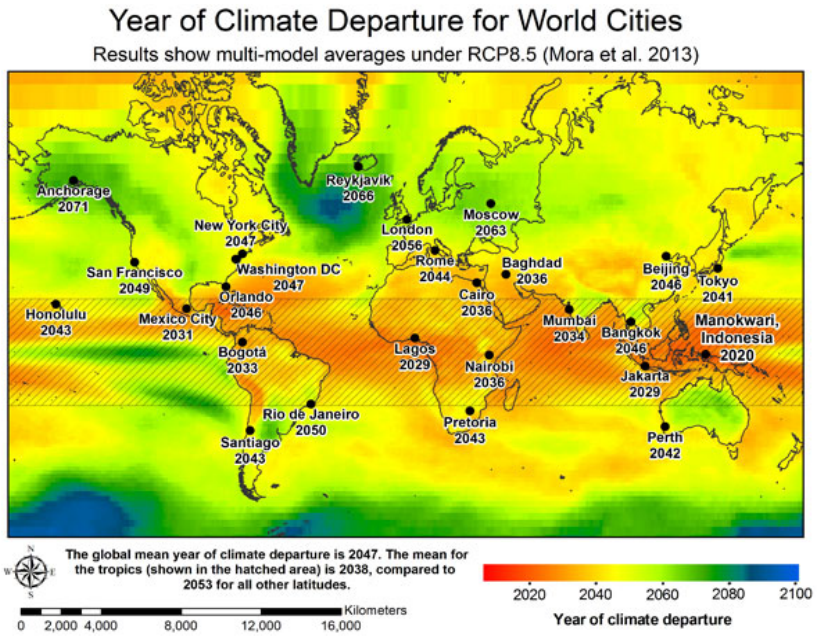

Figure 1.1. Map showing the years of when the low temperature value of major cities around the world would shift by several degrees higher. [2]

gions. This basically means an increase in the frequency and intensity of extreme weather worldwide, and that the top one percent of the heaviest rain or snow storms are heavier now, as reported in Ref. [3]. The IPCC report also mentioned about the increase in tropical cyclone activity in the Western North Pacific and North Atlantic.

Aside from reiterating the physical science basis of climate change in the IPCC report, the US National Research Council also recently reported about the need to create an early warning system for abrupt impacts of climate change [4, 5]. They are looking at "tipping points" for global warming disasters that in theory will happen in the future but are already manifesting risks for "abrupt impacts" like sudden sea-level rise, water shortages, and extinctions worldwide in the coming years and decades. Even though there are apparent trends in climate change already, many scientists still reiterate the need for more climate monitoring projects. Recently, however, there have been declines in funding climate monitoring projects, just when it is needed the most [6].

Of the many changes in climate and weather patterns, it is the recent in-

crease in frequency and intensity of tropical cyclones that is causing much damage through climate-induced natural disasters like floods and landslides. Just recently, Typhoon Haiyan devastated central Philippines and eventually became the deadliest Philippine typhoon on record. It is also the strongest storm to make landfall, and the fourth strongest typhoon ever recorded in terms of wind speed [7]. It is a sign of climate change, however, that for the past four years the Philippines has been experiencing extreme rain events that cause widespread flooding every single year. It is another evidence that weather patterns are changing and consistent monitoring is important, especially in developing countries like the Philippines where there is only a limited number of weather sensors available.

Another factor that makes the Philippines so vulnerable to climate change is that it is a tropical country. Tropics refer to the part of the world that is within the 23° latitude from the equator. Nearly two-thirds of all rain events happen in this region. Economically speaking, most tropical countries are considered developing countries and have less rainfall sensors than one would find in a developed country. Most typhoons also develop in the tropical region. These typhoons form and move faster and require more sophisticated forecasting, something that is hard to do in developing countries. Because of the frequency and intensity of rainfall events, tropical countries are also more susceptible to rain-induced disasters like landslides and flash floods.

The climate in tropical countries is divided into two seasons – rainy and dry – although it is not unusual for these countries to experience rain all throughout the year, even during the summer season. Also, rain events do not necessarily have to be associated with large-scale phenomena like typhoons. In fact, summer rains or rain during a fair weather day is normal in tropical countries. There are several known characteristics of tropical rain as compared to mid-latitude or temperate region rain. Tropical rains not associated with typhoons can still be very intense over a small area and can reach rain rates of more than 200 mm/hr at a time. The cell size of these events can be from sub-kilometer to a few kilometers. They can also last from several minutes to a few hours. Due to these characteristics, tropical rains can trigger disasters like flash floods and landslides. Tropical rains can dump a huge amount of rain in a short period of time, causing the swelling of rivers and drainages. The intense localized rain can also produce enough force

that can drive down the soil and trigger landslides.

Detecting localized tropical rain is hard because it occupies only a small area, and forecasting its occurrence is even harder. There are several ways of detecting and forecasting tropical rain. The most common method is through the use of weather satellites and RADARs (*RA*dio *D*etection *A*nd *R*anging). Meteorological satellites have the advantages of covering the ocean areas for improved forecasting and they can see the start and development of typhoons for improved typhoon warning services. Long-term satellite data are also used to understand the weather and climate patterns for better forecasting. Weather radars, on the other hand, are used to detect the typhoon as it approaches. Radars are capable of calculating the motion of the rain clouds, the type of precipitation (rain, snow, etc.), and the intensity. Weather radar data are important in determining potential severe weather patterns. A disadvantage of satellites and radars, however, is that they are not suitable for ground level rain estimates. The ground level rain data is important to calculate the possible run-off that can cause flash floods and landslides.

One way to get the ground level rain is through the use of local weather stations. These weather stations usually consist of a set of instruments to measure different weather parameters like rain, temperature, pressure, wind speed and direction, and humidity. They take real-time measurements of weather events happening in the specific location where they are deployed. The data from these stations are used to verify the forecasts made using the satellites and radars, and to monitor the current weather conditions in a specific area. A good deployment of weather stations is through a mesonet, which is a network of sensors used to observe weather phenomena in the scale of 5 kilometers to around 1000 kilometers. The distinguishing feature of a mesonet is the station density and temporal resolution. The spatial spread out of weather stations can be from 2 to 40 kilometers, while the temporal resolution is every 1 to 15 minutes. However, mesonet deployment can be very expensive as it depends on the number of stations available, and only some developed countries have permanent mesonet systems. Normally, most weather stations used by other government entities, private companies, and individuals are deployed in the scale of one in every tens of square kilometers. For the purposes of detecting localized tropical rain, which

happens in the sub-kilometer scale, the weather stations normally deployed few and far in between are inadequate.

In Japan, these localized sudden rainfall events are called "guerilla rain" because of the similarities in attack time and intensity. In a Japanese article published online last July 17, 2010, guerilla rain was defined as "sudden downpours into relatively narrow zones, mainly in urban areas." There were reported incidents of deaths in Tokyo and Kobe in 2008 caused by the sudden swelling of rivers and underground tunnels because of guerilla rain [8]. In recent years, more attention is being focused on the detection and forecasting of these rain events. Several mobile phone applications were made available to the public, giving the local area forecast for the next 10, 20, 30, or 60 minutes. These applications make use of data from the Automated Meteorological Data Acquisition System (AMeDAS), an automatic weather observation system that consists of about 1300 stations located all over Japan. Figure 1.2 shows the location of AMeDAS stations in Okinawa, the southern islands of Japan [9].

Figure 1.2. Location of AMeDAS stations in Okinawa, Japan.

There are 17 stations in and around Okinawa Island. The island has an area of around 1200 square kilometers, which means that on average there is one station

for every 70 square kilometers. Each station is also on average 17 kilometers apart from each other. Although this is already an impressive monitoring system, the coverage area is still too large for the purposes of detecting and forecasting guerilla rains.

2 Overview of the Problem

Emerging studies on climate change shows that more and more extreme rain events like Typhoon Haiyan and guerilla rains are happening around the world. Because of this, there is a need for innovative and easy-to-deploy weather measurement systems that can help monitor the weather and climate changes, especially around the tropical region where not much weather sensors are available. The particular type of rain event that we want to detect, the localized heavy rain, is hard to detect using traditional weather sensors because of its size and event duration. However, it can be detected with the use of microwave communication networks. These microwave links are sensitive to rainfall attenuation. By using this information, we can calculate the specific attenuation in a certain area and directly relate it to the rate of rainfall that is happening in that area. However, just using the link attenuation data is not enough because its resolution is low for detecting localized heavy rain.

3 Research Contribution

In this dissertation, the main task is to be able to detect the sporadic heavy rain using the rainfall attenuation of microwave mesh networks. Microwave links are easily affected by rain and its attenuation due to rainfall has been widely discussed in literature. Prediction methods and design models like ITU-R P.530 and the Global Crane Model are usually used in designing microwave networks so they can withstand rain attenuation [10, 11]. Depending on the intensity of a rain event, microwave links suffer a certain amount of signal absorption but they can still function normally as a communication channel. This change in the received signal level, measured over a certain distance, can be used to infer the rainfall rate within the signal path. Matzler, et al., showed the potential of using

directional transmission links to derive the rain rate at a high time resolution and in near-real time [26]. In this research, instead of using individual microwave links, several links in a microwave mesh network are used simultaneously and their link attenuations measured. From this link attenuation, the specific attenuation of a certain area within the link is reconstructed using a new technique called compressed sensing. This technique can reconstruct a signal or an image using a limited number of measurements. The results suggest that microwave mesh networks can be used as weather sensors and are effective in determining the location and intensity of the rain along its path.

4 Research Tasks and Limitations

This dissertation will be discussing about the effects of rainfall on microwave communication networks and how the networks can eventually be used as rain sensors. The first task done was to use real radar rainfall data to simulate the attenuation that a link will experience in different parts of Japan, under different weather conditions. From this task, the effects of rainfall on the placement and design of microwave networks were investigated and route diversity configurations were analysed and evaluated. After this, the next task was to simulate different mesh network configurations with the goal of reconstructing the rainfall field. The results of the reconstruction was compared with the original rainfall data and the accuracy of the method was analysed.

5 Dissertation Layout

The dissertation is organized as follows:

This chapter gives the general introduction for the research. The motivations and overview of the problem were discussed along with the contributions and tasks that this dissertation wishes to achieve. Chapter 2 will discuss the relationship between microwave communication links and rainfall. The use of microwave links as rain sensors will also be discussed. Chapter 3 talks about the route diversity experiments done to show the effect of rainfall attenuation on the outage probability of microwave networks. These experiments were designed based on

the links' orientation and angle of separation from each other. Chapter 4 discusses the rainfall field reconstruction using rain attenuation of the microwave networks. This reconstruction was done using the compressed sensing algorithm. The last chapter gives the conclusion and future works.

Chapter 2

Related Literature

1 Microwave Links Used in Terrestrial Communication Networks

Wireless network deployment has gone up in the last decade all over the world with the development of new technologies and availability of wider markets. People are becoming more mobile and the wireless networks provide the mobility and accessibility that this fast-paced generation demands. Microwave links are the backbone of wireless networks. Microwave radio links use line-of-sight propagation; therefore any obstruction between the transmitters will affect the proper transmission of signals. These links usually operate in the GHz frequencies, which are very susceptible to rain. Rain fades start to become a concern at around 5 GHz and is more evident at frequencies above 10 GHz [11]. Rain is an important factor in determining the link availability and reliability, and a good microwave network design relies heavily on the rain statistics of a particular deployment area. Link designs usually incorporate the expected rain fade into the link budget by following rain attenuation models. Local rain data is preferred for calculations whenever available, but rain rate values are also available in attenuation models like the ITU-R P. 530 and the Crane Global Model.

Link designers take note of the effects of rain on microwave signals mainly for the quality of service. However, studies in the recent years have shown that the same received signal level (RSL) attenuation data can be used as an indicator of

the intensity of the rain along the path of the link [12, 13]. Many studies suggested the use of wireless communication networks for environmental monitoring and used the observations to supplement the data provided by conventional rain sensors [14, 15]. A study by Messer, et al [16], used the wireless communication networks of Israel to monitor and reconstruct the rain fields. Path-averaged rainfall from wireless links has also been the topic of several studies. In a paper by Rahimi, et al [17], they made use of two microwave links from different frequency bands. The difference in attenuation between the two links was used for rain attenuation, and the use of two frequencies resulted in a relatively more linear relationship between attenuation and rain rate, as compared to using only one frequency and then using the exponential power law model to get the rain rate. Meanwhile, Berne and Uijlenhoet showed that the path-averaged rainfall estimation using microwave links has an uncertainty due to the spatial variability of rainfall [18]. This finding is more obvious with tropical rain because individual rain events can have a size as small as a few hundred meters to several kilometers. The movement of rain clouds is also fast such that each event can be passing through the links in only a short period of time.

2 Signal Attenuation Due to Rain

There are several radio propagation models developed to calculate the predicted attenuation due to rain of microwave links. The International Telecommunications Union - Radiocommunication Sector (ITU-R) has a set of standards or recommendations for the calculation of rain attenuation in microwave network design. The ITU-R recommendation, along with another popular radio propagation model called the Crane Global Model, is commonly used by link designers.

The ITU-R recognizes several factors that affect the propagation and must be considered in the design of a line-of-sight link [10]:

- Diffraction fading due to obstruction of the path by terrain obstacles under adverse propagation conditions;
- Attenuation due to atmospheric gases;

- Fading due to atmospheric multipath or beam spreading (commonly referred to as defocusing) associated with abnormal refractive layers;
- Fading due to multipath arising from surface reflection;
- Attenuation due to precipitation or solid particles in the atmosphere;
- Variation of the angle-of-arrival at the receiver terminal and angle-of-launch at the transmitter terminal due to refraction;
- Reduction in cross-polarization discrimination (XPD) in multipath or precipitation conditions;
- Signal distortion due to frequency selective fading and delay during multipath propagation.

When a microwave link has already been set up and the best received signal level has been achieved under local conditions, the only remaining major factor for the link to go down is the presence of precipitation. The main kind of precipitation experienced is rain, therefore in link designs there usually is a rain fade allowance that is between the normal signal level and the receiver sensitivity. Figure 2.1 shows a sample received signal level for a 26 GHz microwave link. The normal received signal levels is at -65 dB while the receiver sensitivity is -79 dB, which gives the link a 14 dB fade margin. Until the receiver sensitivity level, the signal can be received without errors. Errors start to occur between the receiver sensitivity and the minimum received signal level. Beyond the minimum received signal level the link will experience down time, meaning no communication is exchanged between the two transceivers.

Factors that affect the rain fade are rain rate, drop size, drop shape, and drop volume density (number of drops per m^3). Most commonly measured among these factors is the rain rate so it is most often used for fade calculations. There are three ways rain can affect electromagnetic signal transmission. Rain can attenuate the signal, increase the system noise temperature, and change the signal polarization. All of these three degrades the received signal and are dependent on the carrier frequency. As the carrier frequency increases, their effects become increasingly significant [19].

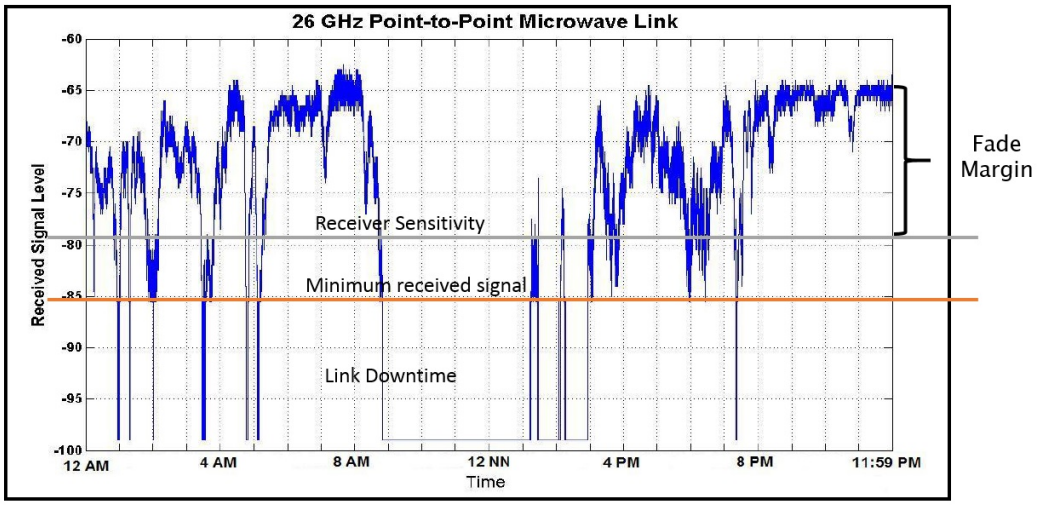

Figure 2.1. Example of fade margin allocation in a microwave link.

Signal attenuation is caused by the scattering and absorption of the electromagnetic signal by the liquid raindrop. Scattering will disperse the signal while absorption will cause some of the signal energy to be absorbed by the drop, causing a slight increase in the temperature of the drop. Attenuation is highest when the wavelength of the signal is the same as the size of the raindrop. Since a raindrop size is only in millimeters or even smaller, similar size wavelength corresponding to GHz frequencies is the most affected electromagnetic band. Of the frequencies used for wireless communication, VHF and UHF bands are almost not affected, and rain attenuation becomes significant starting from the SHF (3 GHz to 30 GHz) band. In the microwave spectrum, rain attenuation starts to get significant in the X band (8-12 GHz). Most microwave communication terrestrial links are in the X, Ku, K, and Ka bands (8-40 GHz) so rain attenuation is an important factor in their design.

There are two widely used models for predicting signal attenuation due to rain: the ITU-R and the Crane Global Model.

2.1 ITU-R Rain Attenuation Model

The ITU-R rain attenuation model specifically for terrestrial line-of-sight microwave links is given by Recommendation ITU-R P.530-10. This model gives the formula for the predicted attenuation due to rainfall based on the desired

availability. Important parameters include specific attenuation, the regression coefficients computed from the ITU data library, and the rain rate. The regression coefficients are dependent on frequency and polarization. Figure 2.2 shows the different regression coefficients for a 50 mm/hr rain.

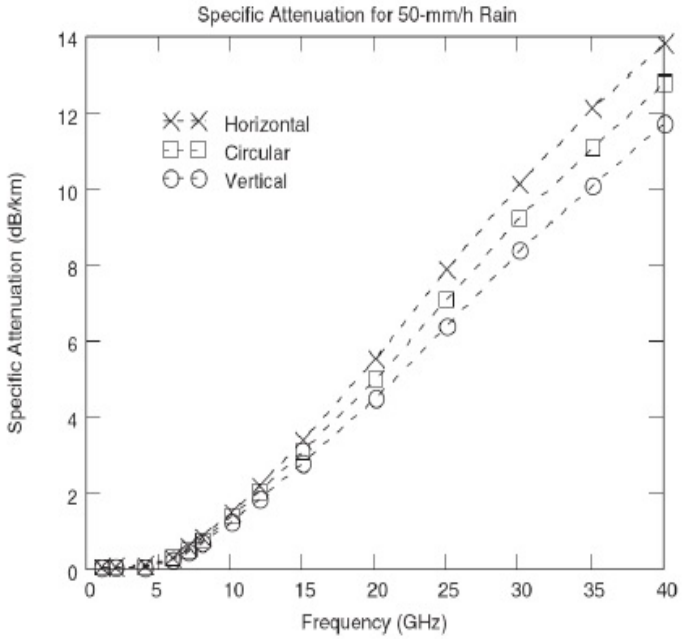

Figure 2.2. Specific attenuation for different frequencies and different polarization.

The specific attenuation is given by

$$\gamma = kR^{\alpha}. \tag{2.1}$$

In this equation, γ is the specific attenuation due to rain in dB/km and R is the rain rate in mm/hr. Constants for the k and α coefficients are developed from scattering calculations and differ in value for different frequencies (1 to 1000 GHz) and polarization (horizontal or vertical). The values for these constants are already given in ITU-R P.838-3. The link attenuation can be calculated by getting the sum of the specific attenuations in a given link path.

To apply the ITU-R method, the first thing to determine is the 99.99% fade

depth using the following formula:

$$Atten_{0.01} = kR^{\alpha}dr \tag{2.2}$$

which is the same as Eq. (2.1) but with the additional parameters d and r. Parameter d is the link distance in kilometer, while r is the distance factor given by:

$$r = \frac{1}{1 + \frac{d}{d_0}} \tag{2.3}$$

where

$$d_0 = 35e^{-0.015R} \tag{2.4}$$

is the effective path length.

$Atten_{0.01}$ will give the expected rain attenuation when the rain rate is equal to the rain rate that occurs only 0.01% of the time. This can equivalently be the rain fade margin when you want a microwave link that is available 99.99% of the time. The $R(0.01)$ rain rate may be obtained directly from local rainfall data, or if not available, it is given in ITU-R P.837-4 [20]. For availabilities other than 99.99%, adjustments need to be done to $Atten_{0.01}$.

$$Atten_p = Atten_{0.01}[0.12p - (0.546 + 0.043\log(p))] \tag{2.5}$$

$$Atten_p = Atten_{0.01}[0.07p - (0.855 + 0.139\log(p))] \tag{2.6}$$

Equation (2.5) is for areas with latitude greater than 30° North or South of the equator, while Eq. (2.6) is for latitudes below 30° North or South of the equator. The variable p is the desired probability (100 - availability) expressed as percentage.

2.2 Crane Global Model

The Crane Global Model was developed by Robert K. Crane. It uses the same regression coefficients as the ITU-R model. The general formula of the Crane

Model is different from that of the ITU-R, as well as the $R(0.01)$ for different regions in the world. The attenuation model is given by:

$$Atten = \begin{cases} \dfrac{kR^{\alpha}(e^{y\delta}-1)}{y}, & \text{for } 0<d<\delta(R) \\ kR^{\alpha}\left(\dfrac{e^{y\delta R}-1}{y} + \dfrac{(e^{zd}-e^{z\delta R})e^{0.83-0.17\ln(R)}}{z}\right), & \text{for } \delta(R)<d<22.5 \end{cases} \tag{2.7}$$

where d is the link distance in kilometer, and

$$\delta(R) = 3.8 - 0.6\ln(R) \tag{2.8}$$

$$y = \alpha\left(\frac{0.83-0.17\ln(R)}{\delta(R)} + 0.26 - 0.03\ln(R)\right) \tag{2.9}$$

$$z = \alpha(0.026 - 0.03\ln(R)) \tag{2.10}$$

The ITU-R model is valid for link distances up to 60 km while the Crane Global Model is valid for link distances up to 22.5 km [11]. In general, the Crane model gives a higher attenuation prediction than the ITU-R model.

2.3 Link Budget

Other factors aside from rain attenuation should be considered in designing a microwave link. The estimated link distance is based on system gain, antenna gain, and propagation effects.

System gain is the maximum average transmit power minus the receiver sensitivity, with formula given by:

$$G_S = P_{Tmax} - R_{thresh} \quad \text{(dB)}. \tag{2.11}$$

Link gain is the system gain plus the sum of the transmitter and receiver antenna gains:

$$G_L = G_S + 2G_{Ant} = P_{Tmax} + 2G_{Ant} - R_{thresh} \quad \text{(dB)}. \tag{2.12}$$

The link gain may be adjusted to account for other losses like mutual interference, multipath, alignment error, atmospheric loss, and others. The free space path loss must also be calculated and taken into account. It is given by:

$$L(d) = 20 \log \left(\frac{\lambda}{4\pi d} \right) \quad \text{(dB)}. \tag{2.13}$$

For the given link distance, d, the available fade margin is the difference between the link gain and free space loss, given by:

$$FM = G_L - L(d) \quad \text{(dB)}. \tag{2.14}$$

This fade margin may be allocated to rain fades and other link impairments.

3 Route Diversity

There are several rain fade mitigation techniques that can be employed to lessen the effect of attenuation on the communication links. The most common ones are route diversity, link separation by a certain angle, and link orientation.

Route diversity is generally defined as the availability of more than one physical path from the source to the sink. This is useful especially when the main communication link is unavailable for reasons like power outage, blockage, or extreme attenuation due to rain. Route diversity gives other options for the information to be routed from the source, choosing other available paths that are usually slower or more costly than the main one. Diversity can be achieved by using totally different technologies that are affected by different disturbances, or by using same technologies but applying site diversity techniques.

Diversity through link separation is achieved by varying the angle between the two links. A source node can transmit the data into two or more relay nodes, and anyone of them can then transfer the data to the sink node. In the case of a rain event, when one of the links is suffering from attenuation, the other links can do the job of transmitting the data. However, if the two links are placed very near to each other with only a small angle between them, the probability of being affected by the same rain event is high. In this case, most probably both of the links will be attenuated at the same level. However, a wider angle between

nodes means less probability of the 2 links being affected by the same rain event. In this case, an angle of 180° between the two relay nodes would give the highest diversity.

4 Rainfall Detection Using Microwave Attenuation

The horizontal profile of a rain event has large spatial variation, with most of the rainwater pouring in the center of the event and gradually dissipates toward the edges. The vertical profile is also variable with different cloud heights, but microwave detection of rain is considered near-ground sensing and is not affected by this variation. The rainfall rate as it passes through the signal is the same as the rate as it falls to the ground. Since microwave links can detect the presence of rain along the link, it is also possible to infer the rain location from the simultaneous attenuation in mesh network. One way to do this is shown in Fig. 2.3. Suppose that there are three criss-crossing microwave links in a 5 km by 5 km area. In a rain event, any of the three links can experience signal attenuation. The location of the rain can be inferred by looking at the path of the link that experienced signal degradation. If two or more links get attenuated at the same time then it is probable that there is a rain cloud large enough to affect several links. The accuracy in detection also increases when the number of links crossing a certain area increases. In the figure, detecting rainfall in Area B will be very accurate when all three links are attenuated at the same time. The area where all three links intersect will always have higher detection accuracy than the other areas where only one link is present. The movement of the rain cloud can also be inferred from looking at the time series attenuation of each link and will have more accuracy when there is available data on wind direction. Given the attenuation of the mesh network, the specific attenuation can be derived using a method called compressed sensing, which is discussed in the next section. Finally, the rainfall rate in an area can be derived from the specific attenuation using Eq. (2.1).

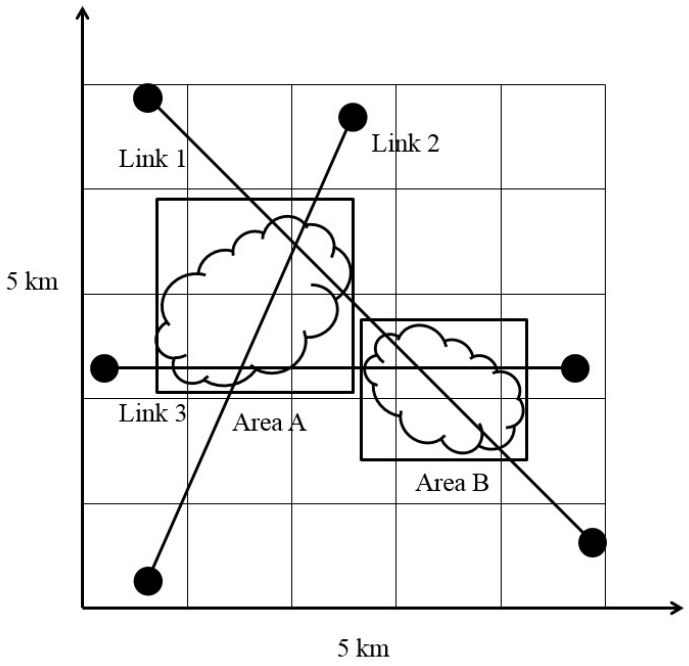

Figure 2.3. Determining rain location from link attenuation.

5 Compressed Sensing Algorithm

Compressed sensing, also referred to as compressive sampling, is a relatively new technique in signal processing that can efficiently acquire and reconstruct a signal through l_1-norm minimization [28,30]. Introduced in 2006, the idea of compressed sensing came at a time when the created global information has started to exceed the available storage. The basic idea was to avoid sampling the part of the signal that will only be lost in compression, therefore needing less storage space, and the sparse image can be accurately reconstructed from lesser samples than traditional methods use. It was first applied in Magnetic Resonance Imaging (MRI) images, and are now commonly applied to areas such as image processing and channel state estimation. It is specifically useful when the data to be reconstructed is sparse in some basis, i.e. mostly negligibly small or zero. It proposes a simple acquisition process followed by numerical optimization.

The digital revolution and widespread use of sensor systems in almost all aspects of life created a huge amount of data that needs to be sampled and stored.

Ideally, a signal must be sampled at twice the highest frequency for an exact recovery, as stated by the Nyquist-Shannon sampling theorem. However, most real world signals have very high frequency content, resulting in large amounts of sampled data. It has been noted, however, that high-frequency content is not necessarily the same as high-dimensional, and that most interesting signals often obey low-dimensional models such as sparsity, low manifold representation, or form low-rank matrices. A key idea of compressed sensing is that many natural signals have representations wherein the "intrinsic dimension" S of the model can be much less than the "ambient dimension" N of the original signal [31]. This also means that the "information bandwidth" is less than the total bandwidth of the signal. Figure 2.4 shows the sample-compress paradigm that is the standard digital data acquisition method nowadays. The continuous time signal x would be sampled at the Nyquist rate N and then compressed to only S numbers, where S is many times lower than N. This S samples can then be transmitted or stored for decompressing later on. This method, however, can be inefficient because acquiring large number of samples can cost money and time. Compressed sensing explores the idea of sampling below the Nyquist rate without information loss by acquiring the S samples directly without having to go through the sampling process, and since the acquisition process has changed, how to recover or process this data by convex optimization for different applications.

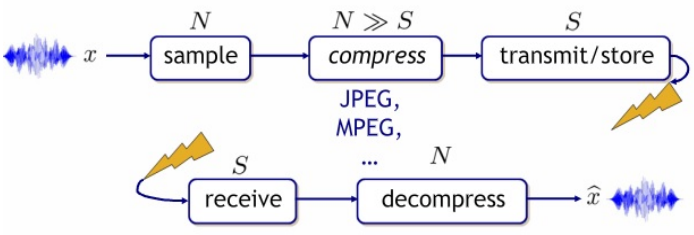

Figure 2.4. Digital data acquisition normally involves sampling then compressing the data before storing or transmitting [31].

Compressed sensing is about sampling in a different way and samples are replaced by general linear measurements. A linear measurement model is commonly given by

$$\mathbf{y} = \mathbf{\Phi x} \tag{2.15}$$

where $\mathbf{y}$ is an M-vector of measurements, $\mathbf{x} = (x_1, x_2, \ldots, x_N)^T$ is the desired sparse unknown N-vector, and $\mathbf{\Phi} = (\Phi_{1,1}, \Phi_{1,2}, \ldots, \Phi_{M,N})$ is an $M \times N$ known measurement matrix. S-sparse means there are S non-zero entries in the vector $\mathbf{x}$. Figure 2.5 shows this in illustration form.

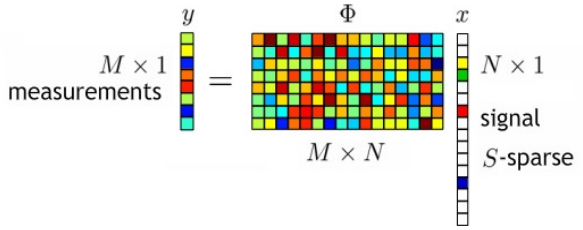

Figure 2.5. Linear measurement model for compressed sensing.

In this particular methodology, the number of measurements is much less than the dimension of the signal, making it an underdetermined system where there are fewer equations than unknowns. Compressed sensing algorithm can be used to solve for $\mathbf{x}$ if $\mathbf{x}$ is determined to have a unique sparse solution. Compressed sensing reconstruction can be done by optimization through l_1-norm minimization or by using greedy algorithms like Matching Pursuit (MP) and Orthogonal Matching Pursuit (OMP).

For compressed sensing to be robust against noise, the sensing matrix $\mathbf{\Phi}$ should be chosen such that it satisfies the condition called Restricted Isometry Property (RIP). The idea of RIP is that for any pair of vectors that are both S-sparse, the matrix $\mathbf{\Phi}$ preserves the distance between them. In Fig. 2.6, x_1 and x_2 are S-sparse vectors in dimension $N = 3$. When Φ is applied to these vectors and mapped in a lower dimension $M = 2$, the distance between these vectors does not change very much (up to $\pm\delta$ as in Eq. [2.16]). This is important because real-world signals when sampled have noises incorporated in them, making the samples close to but not exactly equal to the desired signal. Since compressed sensing is sampling at a much smaller dimension and that reconstruction will be based on these samples, the error is minimized when the sampling matrix satisfies the RIP condition. It is called *restricted isometry property* because we can equivalently write Eq. [2.16] to be Eq. [2.17], where it says that Φ preserves the norm of $2S$-sparse vector. The two equations are equivalent because the difference vector

obtained from the difference between any pair of S-sparse vectors is in itself a $2S$-sparse vector. Therefore, if Φ is restricted to any possible sets of $2S$ columns, then that restricted submatrix will be in approximate isometry.

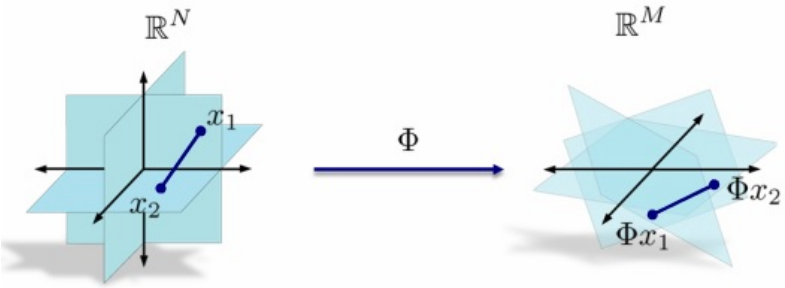

Figure 2.6. The Restricted Isometry Property (RIP) is an important condition of compressed sensing that ensures robustness of the algorithm to noise [31].

$$1 - \delta \leq \frac{||\Phi x_1 - \Phi x_2||_2^2}{||x_1 - x_2||_2^2} \leq 1 + \delta \qquad ||x_1||_0, ||x_2||_0 \leq S \tag{2.16}$$

$$1 - \delta \leq \frac{||\Phi x||_2^2}{||x||_2^2} \leq 1 + \delta \qquad ||x||_0 \leq 2S \tag{2.17}$$

Many researchers argue that RIP is a sufficient condition but not really necessary. Moreover, finding a matrix that satisfies the RIP, or even just checking if any given sensing matrix satisfies the RIP, is computationally impossible. Designing the sensing matrix that definitely satisfies the RIP is therefore hard to do, but there are several ways to construct matrix Φ such that *with high probability* it will satisfy RIP. The simplest method is to randomly choose independent samples from a Sub-Gaussian distribution. For any x, if the entries of Φ are sub-Gaussian, then there exists a δ such that with high probability, Φ preserves the norm of x, as shown in Eq. [2.18].

$$(1 - \delta)||x||_2^2 \leq ||\Phi x||_2^2 \leq (1 + \delta)||x||_2^2 \tag{2.18}$$

Sparse signal, as in Fig. 2.5, will have M equations and N unknowns, where M is many times smaller than N. Signal recovery is therefore difficult, if not impossible, using traditional methods. However, exploring the fact that it is sparse, recovery of the location and values of the non-zeros become potentially

possible. So in Fig. 2.5, all that is known about x is that it is sparse, therefore a logical approach will be to reconstruct x such that the number of non-zeros will be minimized. This is referred to as l_0-norm minimization given in Eq. [2.19].

$$\begin{aligned} \hat{x} = \arg\min_{x \in \mathbb{R}^N} ||x||_0 \\ \text{s.t. } y = \Phi x \end{aligned} \tag{2.19}$$

However, implementing l_0-norm minimization is impossible as it is a non-convex optimization problem. A real breakthrough of compressed sensing came in the form of reconstructing x using the l_1-norm minimization, which is minimizing the sum of the absolute values of the entries in x:

$$\begin{aligned} \hat{x} = \arg\min_{x \in \mathbb{R}^N} ||x||_1 \\ \text{s.t. } y = \Phi x \end{aligned} \tag{2.20}$$

The l_1-norm minimization is a convex problem that can be solved using linear programming. This method works because if Φ satisfies the RIP condition, then l_0-norm and l_1-norm are equivalent.

To apply compressed sensing for rain detection, $\mathbf{y}$ is the RSL attenuation measurement for each link in the mesh network and $\mathbf{x}$ is the unknown or the specific attenuation in a 1 sq. km area. The measurement matrix $\mathbf{\Phi}$ corresponds to the detection area and is defined by the presence or absence of microwave links in a specific location. In the example in Fig. 2.3, there are only 3 links but there are 25 unknown specific attenuations per square kilometer. The spatial diversity of tropical rain is such that most of the time, not the whole area will be covered with rain, making the unknown sparse. Hence, the idea of compressed sensing reconstruction can be applied in the proposed rain detection method. The system configuration and network simulation implementing this algorithm in a mesh network is shown in Chapter 4.

6 Rain Data Used in This Dissertation

The rain data used in this research is the radar data from Japan Meteorological Agency. One set of rain data is for the period of two years (May 2007 to April 2009), with resolution of 1 kilometer by 1 kilometer, taken every 10 minutes.

The other set is for the period of July 2009 to July 2010, with resolution of 1 kilometer by 1 kilometer every 5 minutes. The radar data gives a total of 3360 points vertically and 2560 points horizontally and covers the whole country of Japan.

The specific attenuation of any particular 1 km^2 area can be computed from Eq. (2.1). Subsequently, the link attenuation is computed from the sum of all specific attenuation of the areas where the link passes through.

Chapter 3

Route Diversity Experiments Based on Angular Separation and Link Orientation

This chapter shows how rainfall influences the signal attenuation of microwave communication links. It discusses the attenuation experienced by a 26 GHz microwave link derived from real rainfall data and the route diversity of mesh networks based on the links' angular separation and orientation. With the goal of optimizing the network configuration with proper placement of relay nodes while considering the rainfall attenuation, this chapter looks at how convergent path elements and a simple four-node square configuration of the mesh network will behave under the different rainfall conditions of three locations. The rain data used in this study covers the whole country of Japan, making it possible to choose sites with climates that range from temperate to tropical. The link configurations studied showed significant diversity gain and gave insights about the rainfall behavior in the target areas.

1 Introduction

Microwave links had been the transmission method of choice for broadcasting and telecommunications since its development in the 1950's. Nowadays, microwave is still widely used despite the development of fiber optic communications, which

has become the more dominant transmission method. There are areas where a microwave network is easier to deploy and more economical than installing fiber optic cables, like rural areas and mountainsides.

The microwave link's rainfall attenuation has been widely discussed in literature, while ITU-R P. 530 gives an extensive prediction method for designing terrestrial line-of-sight links [10]. Hendrantoro, et al. [21],used cell-site diversity for fixed cellular systems to resist the effects of rain attenuation. They found that the average correlation of attenuation on two converging links as a function of the angular separation shows the potential benefits of site diversity especially in heavy rain. Shamsan, et al. [22], also studied rain fading mitigation using site diversity for broadband wireless access systems in Malaysia. They showed how switching to the base station without rain can improve the carrier to interference ratio in local multipoint distribution service systems.

ITU-R P. 530 briefly tackles the effects of rain on elements on a route diversity network while ITU-R P. 1410 gives guidelines on the diversity improvement for observed rainfall rates in the United Kingdom [10,23]. Route diversity for microwave mesh networks makes use of the horizontal variability of rainfall, meaning precipitation can change significantly at the sub-kilometer scale. Libatique, et al. [15], showed that for tropical regions like the Philippines, the min-max rainfall ratio in a four kilometer path can be as high as 1:5. In this study, to properly account for this horizontal variability of rainfall, real data from the north, south, east and west directions of a test location were used in determining the diversity gain due to angular separation and link orientation. Using this data, the actual storm movement or rain direction was taken into account, showing how links oriented in one direction behaves relative to links oriented in other directions. Differences due to geographical location were also observed in the specific attenuation experienced by the links. Simple network configurations were studied here and the results can be used to gain insights on how relay nodes can be positioned and oriented in a more complex mesh network.

2 Rain Data and Attenuation

For the purposes of this study, three places that represent different types of climate in Japan were identified. The places are Hokkaido in the higher latitudes, Nara in the central latitudes, and Okinawa in the lower latitudes. Japan's climate is temperate in the north while almost tropical in the south. From each location, four more points in the directions of east, north, west, and south were taken to represent a five kilometer link distance from the center. Figure 3.1 shows the locations and how the points were chosen.

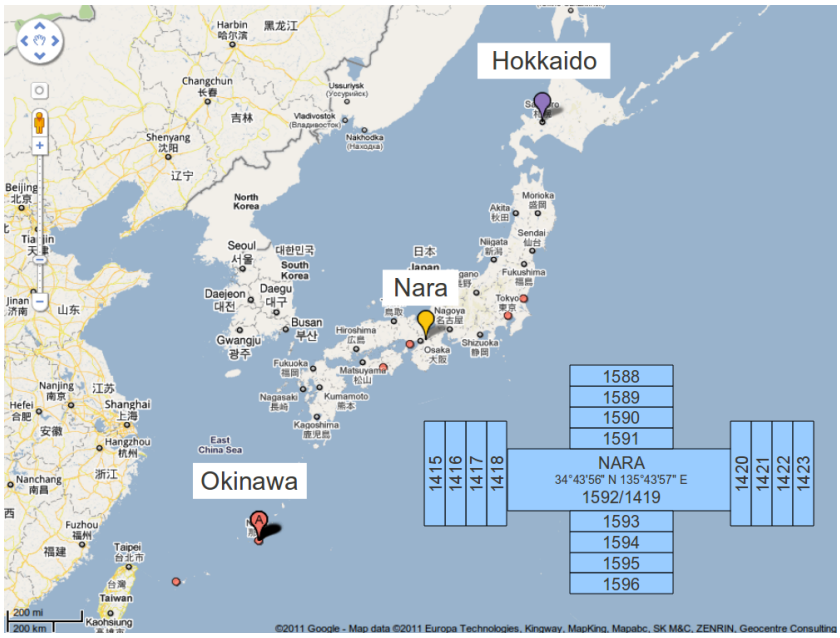

Figure 3.1. Location of the Hokkaido, Nara, and Okinawa test points and the additional points in the north, south, east, and west directions.

The specific attenuation for each 1 km by 1 km data point is calculated from Eq. (2.1) using the following coefficients for a 26 GHz link [25]:

$$\gamma_R = 0.1669 R^{0.9421} \tag{3.1}$$

The link attenuation is the sum of the specific attenuations experienced at each point. In this case, one link attenuation is the sum of the five specific attenuations along its path.

3 Network Configurations

The network configurations for a microwave mesh network considered in this study are the following: (1) convergent path elements and (2) the four-node square configuration. The first configuration is just a part of the whole network, while the second configuration is a simple four-node relay network.

Relay nodes as part of the communication network were first introduced by Van der Meulen in 1971 [24]. The simplest relaying model consists of the source node, the destination node, and a third node that supports the connection between the source and destination nodes denoted as relay node, as shown in Fig. 3.2. If a direct transmission is not possible between the source and destination, the information is forwarded to the relay node to reach the destination by a different path. This method implements the concepts of spatial and temporal diversities. Cooperative communication involves more than one relay node between source and destination. The group of relays can either use space-time codes to transmit, or choose the most reliable relay node while other relays suspend transmission.

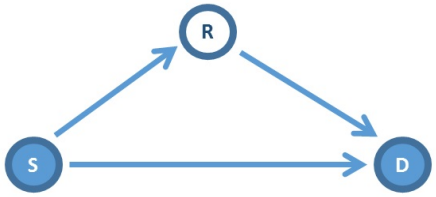

Figure 3.2. Simple three-node relay network with source, relay, and destination nodes.

There are two main relaying protocols: Amplify-and-Forward (AF) and Decode-and-Forward (DF). AF relays are analog and non-regenerative because signals are not decoded before being sent to the destination, only maintaining a fixed average transmit power. On the other hand, DF relays are digital and regenerative because relays decode and encode the signal again before sending it to the destination. The network configurations used in this research follow the AF relay protocol, wherein only the signal strength is considered in transmitting from relay to destination.

3.1 Convergent Path Elements

The convergent path elements configuration, one of the route diversity configurations mentioned in ITU-R P. 530, is characterized by two links meeting at a common node. It was originally developed for point-to-area applications but can also be used as part of point-to-point or multi-hop mesh networks. The diversity improvement in this configuration is due to the links' separation from each other by a certain angle. Because of the horizontal variability of rain, a rain event will not be affecting the two links in exactly the same way, which leads to one of the links experiencing lesser attenuation than the other. Figure 3.3 shows the different angles and orientations considered in this study. There are four 90° and two 180° configurations: East-North (EN), East-South (ES), North-West (NW), West-South (WS), East-West (EW), and North-South (NS). The point of convergence is the information source while the other two nodes are the sinks.

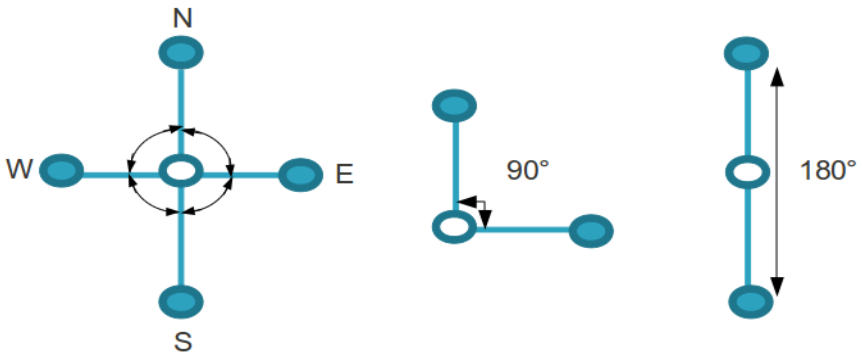

Figure 3.3. Convergent link configurations: 90° (EN, ES, NW, and WS) and 180° (EW and NS).

3.2 Four-node Square Configuration

The next configuration considered in this study is shown in Figure 3.4. The 90° convergent paths previously mentioned can be re-arranged to form two squares with four nodes each. Figure 3.4(a) shows the combination of WS as Route A and EN as Route B to form one mesh network, while Fig. 3.4(b) shows the combination of ES as Route A and NW as Route B to form another mesh network. The information that originates from the source node has two relay nodes that it

can use to deliver the data to the sink node. The source, relay, and sink nodes are labelled accordingly in the figures. The diversity gain in this configuration can be achieved by choosing the route that has a lesser attenuation than the other. The conditions for which route is chosen is explained more in the next section.

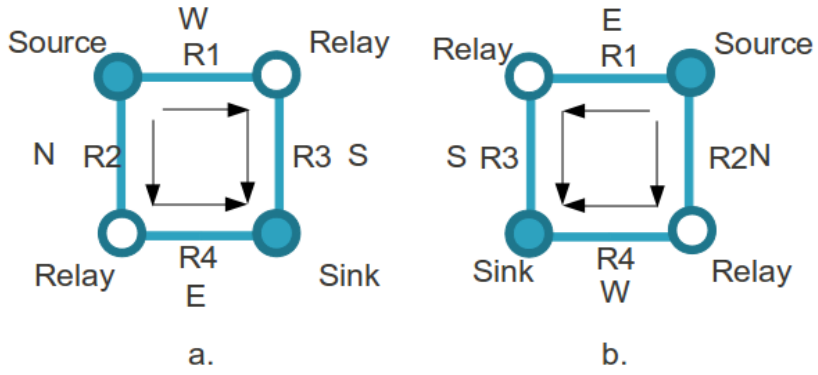

Figure 3.4. Four-node square configurations: (a) Route A: WS, Route B: EN; (b) Route A: ES, Route B: NW.

4 Outage Probability Analysis

To evaluate the route diversity of the network configurations, an analysis on the outage probability was done. For the convergent path elements configuration, the link with the lesser attenuation due to rain will be the diversity path. Because of the spatial variability of rain as discussed in Chapter 2, two links connected to a single node but separated by an angle will experience different attenuations. Applying diversity or choosing the lesser attenuated path would improve the performance of the system as the information travels from the source to the sink. This improvement due to the angular separation may be expressed in two ways: as the diversity improvement $I(A)$ or the diversity gain $G(A)$. ITU-R P. 1410 defines these parameters as follows:

$$I(A) = \frac{P(A)}{P_d(A)} \tag{3.2}$$

$$G(A) = A(t) - A_d(t) \tag{3.3}$$

where $P(A)$ is the time percentage of the unprotected path while $P_d(A)$ is the time percentage of the diversity path, and $A_d(t)$ is the attenuation in the combined diversity path at the time percentage t and $A(t)$ is for the unprotected path.

Figures 3.5, 3.6, and 3.7 show the diversity gain plots for Hokkaido, Nara, and Okinawa. The signal fade depth due to rain for the 10^{-4} percentage of time (without diversity) is the least in Hokkaido at 15 dB, then Okinawa at 35 dB, and the most in Nara at 40 dB.

The effect of angular diversity as measured through diversity gain $G(A)$ and diversity improvement $I(A)$ is also included in the figures. Comparing the diversity gain among the three locations, the highest gain was achieved in Okinawa, followed by Nara, while Hokkaido achieved the least diversity gain. As for the diversity improvement $I(A)$, when comparing the 90° and 180° configurations, the 180° configurations has an obvious advantage because it is the angle that provides the biggest separation between the links. On average, Hokkaido has the highest diversity improvement of the three places, followed by Nara, and then Okinawa. Based on diversity improvement, the NS orientation is favored in Hokkaido, while the EW orientation is favored in Nara. For Okinawa, however, both NS and EW orientations have almost the same diversity improvement.

For the four-node square configuration, the outage probability of one route was calculated by taking the maximum between the attenuations experienced by the two links. The route with the lesser attenuation is then chosen as the diversity path. Tables 3.1 - 3.3 show the values of the attenuation and the fade depth at the diversity path for different percentages of time for the three points. It gives first the attenuation per route and then the attenuation when route diversity is implemented.

5 Discussion

The availability of two years worth of rain data for the whole of Japan enabled us to make some preliminary observations regarding the rain and attenuation characteristics of the three chosen points within the country. The differences

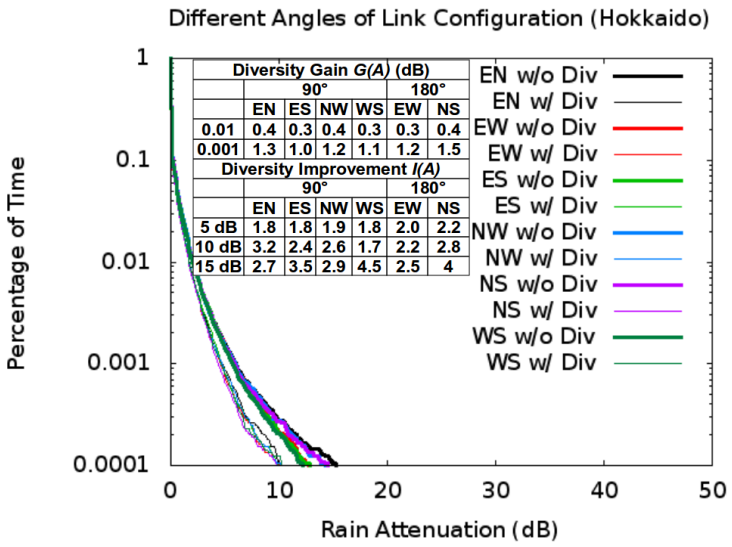

Diversity Gain $G(A)$ (dB)	90°				180°	
	EN	ES	NW	WS	EW	NS
0.01	0.4	0.3	0.4	0.3	0.3	0.4
0.001	1.3	1.0	1.2	1.1	1.2	1.5

Diversity Improvement $I(A)$	90°				180°	
	EN	ES	NW	WS	EW	NS
5 dB	1.8	1.8	1.9	1.8	2.0	2.2
10 dB	3.2	2.4	2.6	1.7	2.2	2.8
15 dB	2.7	3.5	2.9	4.5	2.5	4

Figure 3.5. Diversity gain $G(A)$ and diversity improvement $I(A)$ for Hokkaido.

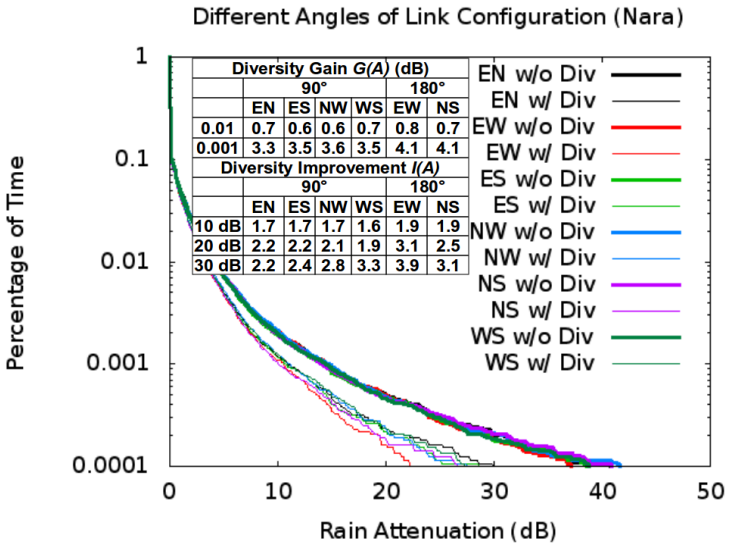

Diversity Gain $G(A)$ (dB)	90°				180°	
	EN	ES	NW	WS	EW	NS
0.01	0.7	0.6	0.6	0.7	0.8	0.7
0.001	3.3	3.5	3.6	3.5	4.1	4.1

Diversity Improvement $I(A)$	90°				180°	
	EN	ES	NW	WS	EW	NS
10 dB	1.7	1.7	1.7	1.6	1.9	1.9
20 dB	2.2	2.2	2.1	1.9	3.1	2.5
30 dB	2.2	2.4	2.8	3.3	3.9	3.1

Figure 3.6. Diversity gain $G(A)$ and diversity improvement $I(A)$ for Nara.

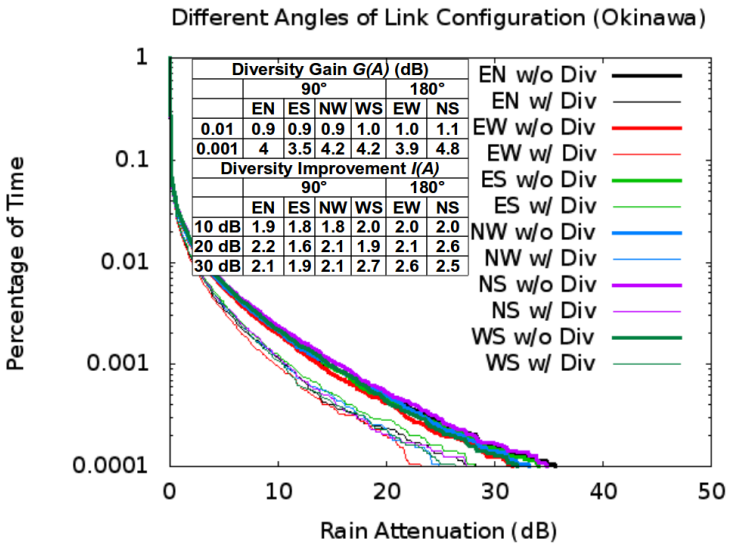

Figure 3.7. Diversity gain $G(A)$ and diversity improvement $I(A)$ for Okinawa.

Table 3.1. Attenuation (dB) of Four-node Square Configurations in Hokkaido

	Route A: ES	**Route B: NW**	**Diversity Path**	**Route A: WS**	**Route B: EN**	**Diversity Path**
0.1	0.2	0.3	**0.1**	0.2	0.3	**0.1**
0.01	2.3	2.4	**2**	2.3	2.4	**2**
0.001	6.7	7	**5.4**	6.6	7.2	**5.4**
0.0001	15.4	16.1	**11.2**	13.8	16.7	**12.2**

Table 3.2. Attenuation (dB) of Four-node Square Configurations in Nara

	Route A: ES	**Route B: NW**	**Diversity Path**	**Route A: WS**	**Route B: EN**	**Diversity Path**
0.1	0.3	0.3	**0.1**	0.3	0.3	**0.1**
0.01	4.7	4.8	**3.9**	4.8	4.9	**4**
0.001	16.8	17.4	**13.4**	17	17.1	**12.9**
0.0001	42.4	48.1	**37**	47.3	45.9	**32.1**

Table 3.3. Attenuation (dB) of Four-node Square Configurations in Okinawa

	Route A: ES	**Route B: NW**	**Diversity Path**	**Route A: WS**	**Route B: EN**	**Diversity Path**
0.1	0	0	**0**	0	0	**0**
0.01	4.1	4	**2.9**	4.3	4.1	**3**
0.001	16.8	17.8	**12.7**	17.5	17.3	**13.7**
0.0001	40.2	37.2	**28.8**	37.2	40.2	**31.1**

between the three sites can be expected primarily because of the different latitudes and prevailing weather conditions. Figure 3.8 shows the rain rate levels of the three points. It can be seen in the figure that Hokkaido has very low rain rate, probably because snow is the main form of precipitation experienced in that area. Before the 10^{-4} mark, the rain rate in Okinawa is stronger than that in Nara. However, after that, Nara gets the more intense but rarer rain events.

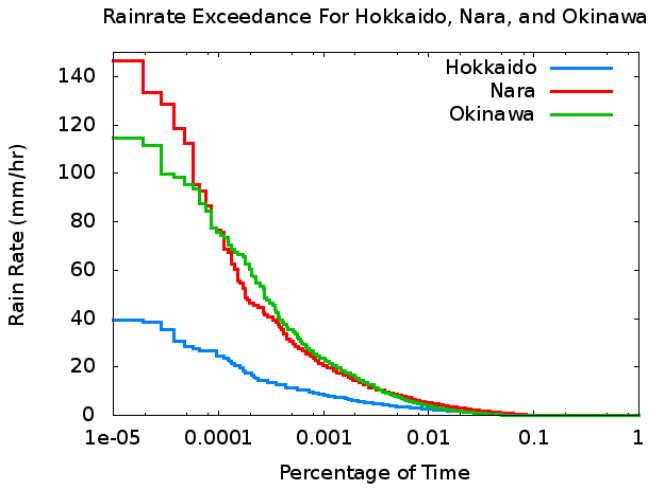

Figure 3.8. Rain rate levels in Hokkaido, Nara, and Okinawa.

For the convergent links configuration, an attenuation event is defined in this study as the time when rain is experienced in one or both of the links. It was observed that Hokkaido has the most number of attenuation events but the overall attenuation is very low. This means that most of the events in Hokkaido have only one link with rain while the other link does not. This also explains why

Hokkaido has a high diversity improvement even for configurations with only 90° angular separations, because the probability that the other link has rain is low. As for the low value of diversity gain in Hokkaido, it can be argued that the attenuation is low to begin with, so not much diversity gain can be achieved with the implementation of path diversity.

In contrast with Hokkaido, Okinawa has the highest diversity gain and the lowest diversity improvement for the convergent paths. Being almost in the tropical region, the rain characteristics in this area is similar to that of the tropics. It can be seen from Fig. 3.8 that for most of the time, Okinawa has a higher rain rate than the other two sites. From the rain data, it was observed that Okinawa experiences rain almost all the time except for the winter months of December to February. The high diversity gain means that the rain is localized like that in Hokkaido, but it has a higher intensity that leads to a higher attenuation, so it gets a lower diversity improvement.

Nara, being in the central latitude, is also between Hokkaido and Okinawa in terms of diversity gain and improvement. Among the three, Nara's outage probability is almost the same for all convergent link orientations. This implies that for the Nara area, the links experience almost the same amount of rain. This means a non-localized rain cell with varying intensities. From the rain data, the seasonal characteristic of rain is very evident for Nara because there is a significant peak in attenuation for the summer months and then minimal attenuation due to rain for the rest of the year. In designing microwave links for areas like Nara, looking at the year's worst month for rain may be more efficient than looking at the yearly data.

For all three sites, the diversity gain and diversity improvement are highest for the 180° link configurations. This is because these configurations have the biggest angle of separation and therefore the lowest probability for both links to experience the same rain event at the same time.

For the four-node square configurations, there is a significant diversity gain in all three sites. It should be noted that the link combinations used for the two square configurations follow the real orientation of the links. The first configuration compares the ES path with the NW path, while the second configuration compares the WS path with the EN path. The attenuation relationship between

the paths is based on real rate data that passes that particular link orientation. It can also be observed that between Routes A and B, the route with the South link orientation is favored. This may mean that out of the four main directions, the south link experiences the least rain with respect to the other links.

6 Conclusion

Mesh network configurations are common when designing microwave networks. It is therefore important to study the effects of rain attenuation in this setting to be able to optimize the placement of relay nodes. The use of local rain data is essential to be able to see the real characteristics of rain in a region for a better estimation of rain attenuation. The route diversity using the link's orientation and angular separation discussed in this study shows the comparison between different link orientations and the simple four-node configuration. There was a significant diversity gain even for a two-hop relay, with preference on the path that includes a south-oriented link.

Chapter 4

Rainfall Field Reconstruction Using Rain Attenuation of Microwave Mesh Networks

The microwave networks' received signal level is affected mainly by rainfall attenuation. The microwave links are usually designed with an appropriate rain fade margin to allow for sudden changes in the signal level and still be able to provide the necessary communication line. Because of this sensitivity to rainfall, commercial communication links has the capability to detect the presence of rain happening in the area where they pass through. A rainfall detection system using commercial communication links can complement the existing weather satellite and radar systems.

This study proposes using the link attenuation of a microwave mesh network to reconstruct the rain field in a 25 square kilometer area using a compressed sensing-based algorithm. Compressed sensing is a new algorithm that can reconstruct a sparse signal from a relatively small number of measurements. Using the link attenuation data from these networks as input to the compressed sensing algorithm, the specific attenuation can be derived. The specific attenuation is directly related to rain rate, as discussed in Chapter 2, so the rainfall field of the 25 square kilometer area can be reconstructed.

From the RADAR rainfall data, the corresponding attenuation of several network configurations were simulated and reconstructed under the proposed

method. The number of links available in a network and their positions relative to each other affects the overall accuracy of reconstruction in an area. Furthermore, increasing the number of links crossing a single location can also improve the reconstruction in that specific location. System configurations wherein the whole 25 points were covered by at least one microwave link as well as configurations that only partially cover the area are investigated and compared. The accuracies of detecting the rain location and attenuation level are evaluated by taking the root mean square error, false positive rate, and false negative rate. Network simulations were done using actual rain data and results show that even for different rain intensities, the rain location and corresponding specific attenuation can be effectively determined. The actual and reconstructed specific attenuation values are compared and the resulting error is practically negligible. The proposed method is also tested for different climate and weather patterns. Moreover, the method can detect extreme rain events that can lead to disasters. The study has possible applications on rain detection and forecasting, identification of the location of extreme rain events without having to use conventional weather sensors, and in designing rain-induced-disaster warning and response systems.

1 Introduction

The novel method of detecting rain using microwave links has been proposed in the last few years. Signal attenuation due to rain is the main problem of wireless communication networks above 10 GHz. In these frequency bands, the radio frequency signal is absorbed mainly by raindrops with the same drop size as the wavelength of the signal. There are several advantages of using microwave links as rain sensors. First, the microwave links are already deployed for commercial communication purposes, and real-time attenuation data is measured as part of the monitoring and maintenance of these links. This means that not much overhead cost is needed to build a rain sensor using the same network. Second, the spatial and temporal resolutions are greatly improved with the use of microwave links. The effective coverage area of the links fit the size of the rain clouds and the observations are made continuously, sometimes in per second resolution. Lastly, deployed microwave links are designed to tolerate rain by a certain fade margin.

Within this margin, the received signal level (RSL) varies with respect to external disturbances, which is mostly rainfall. As long as the RSL does not reach the minimum receiving level of the antenna, the system can record the attenuation due to rain at any given time. The attenuation and rain rate relationship is given by an empirical power-law equation commonly used for link design [35].

Prediction methods and design models like ITU-R P.530 and the Global Crane Model are usually used in designing microwave networks to withstand rain attenuation. Microwave links experience a certain amount of signal absorption depending on the intensity of a rain event but they can still function normally as a communication channel. This change in RSL measured over a certain distance can be used to infer the rainfall rate within the signal path. Matzler, et al., showed the potential of using directional transmission links to derive the rain rate at a high time resolution and in near-real time [26].

Recent research has shifted from determining the rainfall rate from one link to reconstructing the rainfall field using the attenuation data from several links. This study proposes a compressed sensing-based method for detecting the rainfall location and intensity from the attenuation data of microwave mesh networks. Compressed sensing is a new technique that can reconstruct a signal or image using a limited number of measurements [32]. This is useful for rain detection because there are only a limited number of attenuation measurements over an area of several kilometers. Another characteristic of tropical rain is that the rain rate in surrounding areas is usually very much smaller than that in the affected area. This makes the data sparse, which is another requirement for compressed sensing [29].

2 Rainfall Field Detection and Reconstruction

To be able to determine rain location, we propose using the signal attenuation of a microwave mesh network to derive the rain rate in a specific area. The link's attenuation is essentially the sum of the specific attenuations for every kilometer of the link. The specific attenuation is directly related to rain rate as given in Eq. (2.1), therefore if the specific attenuation is known, the rainfall field can be reconstructed. In this research, we propose the use of a compressed sensing-based

algorithm to reconstruct the specific attenuation values from the link attenuation measurements. When first introduced in [28] and [29], the theory's main idea was to avoid sensing/sampling the part of the data/signal that will be lost anyway during compression. The theory asserts that an original "sparse" signal/image can be accurately reconstructed from far fewer samples or measurements than traditional methods use [30]. In compressed sensing reconstruction, we have as input the measurements or samples given by y, the measuring matrix given by Φ, and the output x or the sparse signal that we need to recover. The number of measurements is much less than the dimension of the signal, making it an underdetermined system. An underdetermined system has fewer equations than unknowns and can be solved using non-linear regularization. Compressed sensing makes use of l_1-norm minimization, which can be solved using linear programming.

How to generate the measurements y and use compressed sensing to recover x in the case of rain sensing is shown in Fig. 4.1. To simulate a microwave mesh network and its attenuation due to rain, a 5 km by 5 km area was chosen and a specific number of links was placed on it. The rain rate data used is from Japan Meteorological Agency's RADAR data, with a resolution of 1 km by 1 km for every 5 minutes. For this research, the rain data is from July 2009 to July 2010 to account for all the seasonal changes. For every instance that the 25 km^2 area has rain of any amount, the 25 specific attenuation values were computed using Eq. (2.1). In this study, 25 GHz vertically polarized links were used, and the value of k is 0.1533 and the value of α is 0.9491 [10]. The rain rate is given in mm/hr. The link attenuation can then be computed by adding the specific attenuations along the path of the link, or multiplying the specific attenuation values by the measurement matrix Φ. The specific measurement matrix used is discussed in more detail in the succeeding sections.

To apply compressed sensing for rain detection, $\mathbf{y}$ is the RSL attenuation measurement for each link in the mesh network and $\mathbf{x}$ is the unknown or the specific attenuation in a 1 sq. km area. The measurement matrix Φ corresponds to the detection area and is defined by the presence or absence of microwave links in a specific location. The system configuration and network simulation implementing this algorithm in a mesh network is shown in the next section.

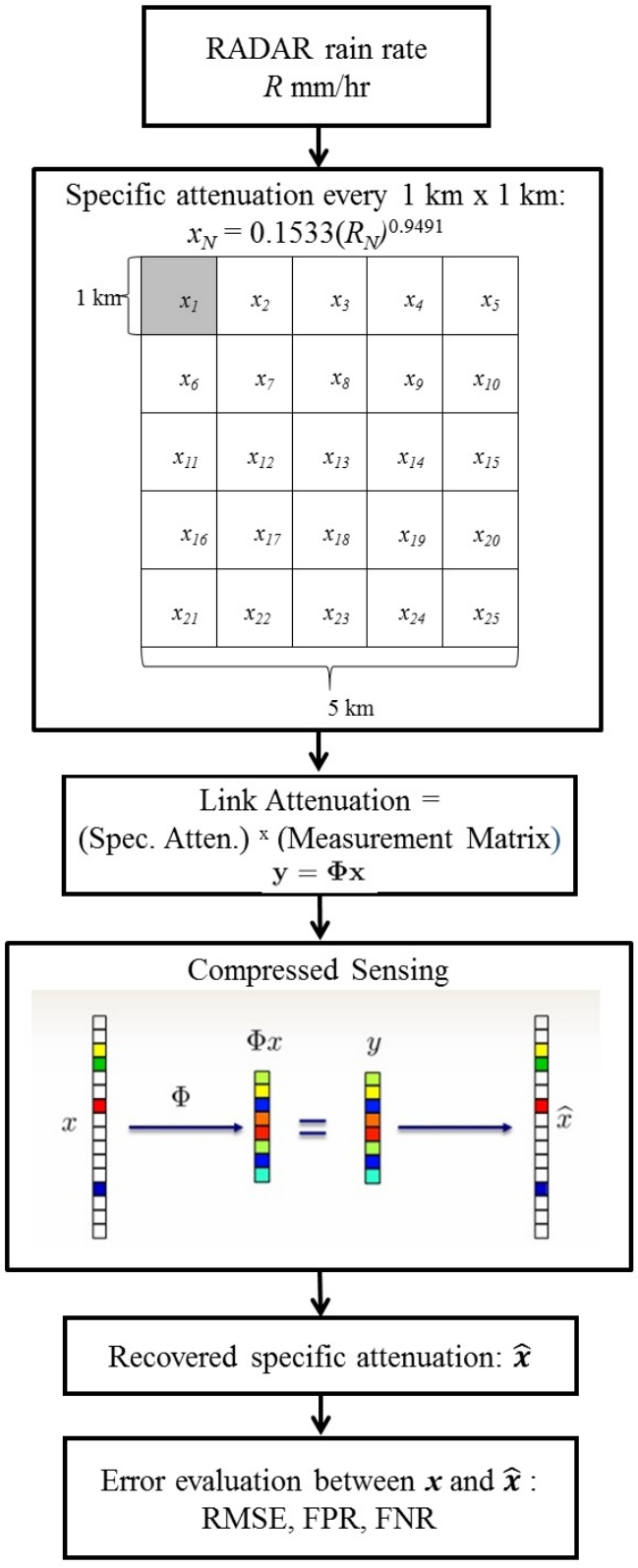

Figure 4.1. Reconstructing the specific attenuation using compressed sensing algorithm.

3 Network Configurations for Fully-covered 25-point Area

For the fully-covered 25-point area configurations, Figures 4.2 and 4.3 show the microwave network placements in the 25 square kilometer area. We can see that in Fig. 4.2, there are two crossing links for every 1 km × 1 km point for a total of 10 links in the area, while for 4.3 there are three crossing links per point for a total of 19 links.

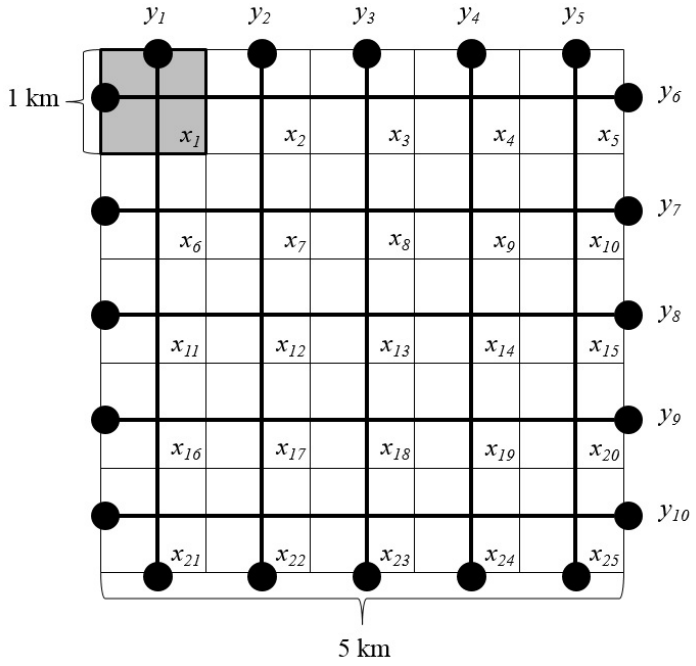

Figure 4.2. Microwave mesh network with two links per area.

Initially, the values for x_1 to x_{25} are calculated using Eq. (2.1) and the link attenuation is calculated from the specific attenuations in the following manner:

$$\begin{bmatrix} y_1 \\ \vdots \\ y_m \end{bmatrix} = \Phi \begin{bmatrix} x_1 \\ \vdots \\ x_{25} \end{bmatrix}. \tag{4.1}$$

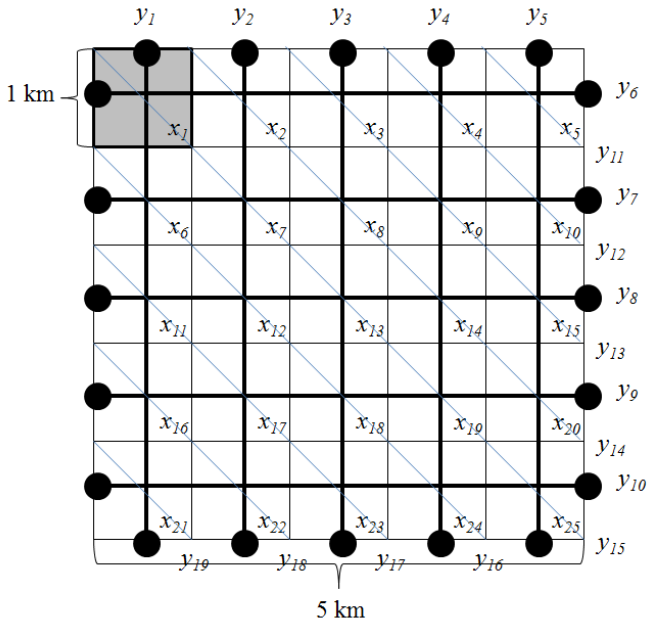

Figure 4.3. Microwave mesh network with three links per area.

For the 10-link configuration, Φ_{10} is given by

$$\Phi_{10} = \begin{bmatrix} 1 & 0 & 0 & 0 & 0 & 1 & 0 & 0 & 0 & 0 & 1 & 0 & 0 & 0 & 0 & 1 & 0 & 0 & 0 & 0 & 1 & 0 & 0 & 0 & 0 \\ 0 & 1 & 0 & 0 & 0 & 0 & 1 & 0 & 0 & 0 & 0 & 1 & 0 & 0 & 0 & 0 & 1 & 0 & 0 & 0 & 0 & 1 & 0 & 0 & 0 \\ 0 & 0 & 1 & 0 & 0 & 0 & 0 & 1 & 0 & 0 & 0 & 0 & 1 & 0 & 0 & 0 & 0 & 1 & 0 & 0 & 0 & 0 & 1 & 0 & 0 \\ 0 & 0 & 0 & 1 & 0 & 0 & 0 & 0 & 1 & 0 & 0 & 0 & 0 & 1 & 0 & 0 & 0 & 0 & 1 & 0 & 0 & 0 & 0 & 1 & 0 \\ 0 & 0 & 0 & 0 & 1 & 0 & 0 & 0 & 0 & 1 & 0 & 0 & 0 & 0 & 1 & 0 & 0 & 0 & 0 & 1 & 0 & 0 & 0 & 0 & 1 \\ 1 & 1 & 1 & 1 & 1 & 0 & 0 & 0 & 0 & 0 & 0 & 0 & 0 & 0 & 0 & 0 & 0 & 0 & 0 & 0 & 0 & 0 & 0 & 0 & 0 \\ 0 & 0 & 0 & 0 & 0 & 1 & 1 & 1 & 1 & 1 & 0 & 0 & 0 & 0 & 0 & 0 & 0 & 0 & 0 & 0 & 0 & 0 & 0 & 0 & 0 \\ 0 & 0 & 0 & 0 & 0 & 0 & 0 & 0 & 0 & 0 & 1 & 1 & 1 & 1 & 1 & 0 & 0 & 0 & 0 & 0 & 0 & 0 & 0 & 0 & 0 \\ 0 & 0 & 0 & 0 & 0 & 0 & 0 & 0 & 0 & 0 & 0 & 0 & 0 & 0 & 0 & 1 & 1 & 1 & 1 & 1 & 0 & 0 & 0 & 0 & 0 \\ 0 & 0 & 0 & 0 & 0 & 0 & 0 & 0 & 0 & 0 & 0 & 0 & 0 & 0 & 0 & 0 & 0 & 0 & 0 & 0 & 1 & 1 & 1 & 1 & 1 \end{bmatrix}. \quad (4.2)$$

For the 19-link configuration, Φ_{19} is given by

$$\Phi_{19} = \begin{bmatrix} & & & & & & & & & & & & \Phi_{10} & & & & & & & & & & & & \\ 0 & 0 & 0 & 0 & 1 & 0 & 0 & 0 & 0 & 0 & 0 & 0 & 0 & 0 & 0 & 0 & 0 & 0 & 0 & 0 & 0 & 0 & 0 & 0 & 0 \\ 0 & 0 & 0 & 1 & 0 & 0 & 0 & 0 & 0 & 1 & 0 & 0 & 0 & 0 & 0 & 0 & 0 & 0 & 0 & 0 & 0 & 0 & 0 & 0 & 0 \\ 0 & 0 & 1 & 0 & 0 & 0 & 0 & 0 & 1 & 0 & 0 & 0 & 0 & 0 & 1 & 0 & 0 & 0 & 0 & 0 & 0 & 0 & 0 & 0 & 0 \\ 0 & 1 & 0 & 0 & 0 & 0 & 0 & 1 & 0 & 0 & 0 & 0 & 0 & 1 & 0 & 0 & 0 & 0 & 0 & 1 & 0 & 0 & 0 & 0 & 0 \\ 1 & 0 & 0 & 0 & 0 & 0 & 1 & 0 & 0 & 0 & 0 & 0 & 1 & 0 & 0 & 0 & 0 & 0 & 1 & 0 & 0 & 0 & 0 & 0 & 1 \\ 0 & 0 & 0 & 0 & 0 & 1 & 0 & 0 & 0 & 0 & 0 & 1 & 0 & 0 & 0 & 0 & 0 & 1 & 0 & 0 & 0 & 0 & 0 & 1 & 0 \\ 0 & 0 & 0 & 0 & 0 & 0 & 0 & 0 & 0 & 0 & 1 & 0 & 0 & 0 & 0 & 0 & 1 & 0 & 0 & 0 & 0 & 0 & 1 & 0 & 0 \\ 0 & 0 & 0 & 0 & 0 & 0 & 0 & 0 & 0 & 0 & 0 & 0 & 0 & 0 & 0 & 1 & 0 & 0 & 0 & 0 & 0 & 1 & 0 & 0 & 0 \\ 0 & 0 & 0 & 0 & 0 & 0 & 0 & 0 & 0 & 0 & 0 & 0 & 0 & 0 & 0 & 0 & 0 & 0 & 0 & 0 & 1 & 0 & 0 & 0 & 0 \end{bmatrix}. \quad (4.3)$$

Here, the measurement matrix defines where the links are located. Therefore, the link attenuation y is the sum of the specific attenuations in areas where that link passed through. These link attenuation values were then used in the compressed sensing-based reconstruction of the specific attenuation. Equation (2.20) is a linear programming problem that can be solved through Matlab. In addition to the given constraints, the lower and upper bounds of x were defined as follows:

$$0 \leq x \leq 25. \quad (4.4)$$

These boundaries were chosen because a microwave link cannot record a negative attenuation and also attenuation beyond the fade margin. The fade margin is the allowance set during the link design phase that will enable the link to still function properly even though the signal is attenuated by rainfall. The normal fade margin value is around 25 dBm.

The rain data used was from Okinawa, Japan. This site was chosen because Okinawa is in the region with subtropical climate and experiences rain all throughout the year because it is in the usual typhoon path. Of the one year data, 11% has rain events on which the proposed reconstruction method was done. The measured link attenuation is an integrated attenuation over the link path, thus the link will register attenuation even if only one part has rain. All kinds of rainfall from very light to violent rain were considered, and the rain cloud size varied from localized to widespread rains. There are 12,645 instances in time that the 25 sq. km. area has rain, regardless of rain cloud size, therefore a total of 316,125 data points were reconstructed.

The reconstruction can be evaluated either as a *false positive* or a *false negative*. The *false positive rate* gives the proportion of reconstructed locations that have non-zero computed rain rates when there is zero rain in the actual data. On the other hand, the *false negative rate* is the proportion of the reconstructed locations with no computed rain rates when in fact there should be. This can be considered as the No Rain threshold, which takes into account only the presence or absence of rain. The false positive rate for the case of 2 crossing links is 9.6% or 30,378 data points, while the false negative rate is 1.3×10^{-4}% or only 41 data points. The high false positive rate can be attributed to the spreading of the specific attenuation into neighboring areas during the reconstruction process. Figure 4.4 shows an illustration for this. The reconstructed area shows some small rain rate in areas where there is no rain in the original data (upper left-hand side). However, the high false positive rate is not a major problem because the reconstructed specific attenuations are very small such that the corresponding rain rate is also negligible. This small amount of attenuation is usually not noticed in real-time monitoring of the links. On the other hand, the very low false negative rate means that the proposed method was able to detect more than 99.999% of the rainfall areas.

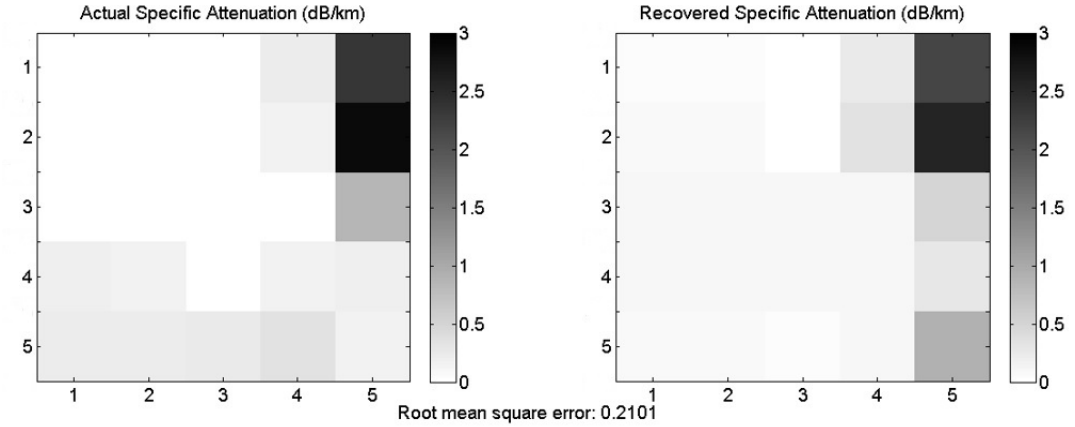

Figure 4.4. Recovered specific attenuation that causes high false positive rate.

The same process can be done for the case of the three links crossing a single area. From Fig. 4.3 it can be seen that there are a total of 19 links in the 25 sq. km. area. The link attenuation input to the compressed sensing algorithm is

Table 4.1. Comparison of RMS Errors Between 2-Link and 3-Link Network Configurations

Rain Rate (mm/hr)	**Spec. Atten. (dB/km)**	**# of Data Points**	**RMSE (2 Links)**	**RMSE (3 Links)**
No Rain	0	148,483	0.06	0.02
Light (<2.5)	<0.40	105, 761	0.11	0.06
Moderate (2.5 - 10)	0.40 - 1.46	49, 801	0.27	0.16
Heavy (10 - 50)	1.46 - 6.65	11, 536	0.77	0.46
Violent (>50)	>6.65	544	2.37	1.27

derived the same way as Eq. 4.3, and this will again be the input for the Matlab program, with the same lower and upper bounds as before. The simulation results verified that increasing the number of links in an area will increase the accuracy of detection. The false positive rate for the case of 3 crossing links is 4.03% while the false negative rate is 5.7×10^{-5}% or only 18 data points.

Aside from the rain location, the proposed method can also reconstruct the magnitude of the specific attenuation, which in turn indicates the rain rate in that area. To evaluate the magnitude reconstruction, the data were divided into 5 categories with respect to rain intensities: no rain, light, moderate, heavy, and violent rain [33]. Table 4.1 lists the categories and their corresponding specific attenuation. The number of data points in the original data set that satisfy each category are counted and compared to the reconstructed values. The root mean square errors (RMSE) for both the 2-link and 3-link reconstructions were also given.

The number of data points per rain rate category indicates the number of times that rain rate was seen in the 25 km square area for the whole data set. There are a total of 12, 645 instances with rain, bringing to a total of 316, 125 data points. As can be seen in Table 4.1, the data points decrease with increasing rain rate because the heavy and violent rains are less likely to happen than the light rains. Also, as mentioned before, even if only one part of the whole area has rain, all of the 25 points will be considered. This is the reason why there are a significant number of data points that have no rain. Since the specific attenuation due to rain was calculated straight from Eq. (2.1), the areas with no recorded

rain are given a corresponding specific attenuation of 0 dB/km. This does not mean that the area does not suffer from any attenuation, only that it does not suffer any attenuation due to rain at that point in time.

From the results in Table 4.1 it can be seen that the proposed method can estimate the magnitude of the specific attenuation very well. The first two categories compose 80% of the data and they have very small errors. Moreover, these rain rates generally do not pose any risk. Moderate rain composes 15.75% of the data and its RMS error of 0.2701 for the 2-link case and 0.1636 for the 3-link case can still be considered negligible because the moderate rain rate in the actual data would still be reconstructed as moderate rain. Heavy rain, which can cause specific attenuations up to 6.65 dB/km, is only 3.6% of the whole data set. Reconstruction for this category has a 0.7724 error. The violent rain category, which comprises 0.17% of the data, has the biggest error of 2.3699. These errors are caused by the reconstruction process's normalization of peak values to the neighboring areas. High specific attenuation values in the original data get distributed to other areas during recovery, causing a decrease in the recovered value. It is however important to note that the largest values from heavy rain and violent rain categories are most probably surrounded by other peak values, causing the overall link attenuation to be almost equal or more than the fade margin. When a microwave link's received signal level goes beyond the receiver sensitivity, it will also have reached the maximum attenuation that it can record. In this regard, determining the location of the peak attenuation is more practical than verifying the accuracy of the recovery.

Figures 4.5 to 4.7 show some examples of the rain area location detection in terms of specific attenuation. For the horizontal axis, the rainfall at the p-th area out of 25-point areas at the time $5q$-minute corresponds to the index

$$i = p + 25q \tag{4.5}$$

Figures 4.5 and 4.6 show detection on different rain regions. It is obvious from these two examples that the proposed method can effectively identify the location of rain. The error in Fig. 4.5 is very small, and it was able to detect the light rain very well. In fact, the reconstruction was also able to show the length of the rain event. For the first five minutes (1-25, q=0), it can be seen that only one

part of the 25-point area has rain. In the next 5 minutes (26-50, q=1), the rain has become more widespread and stronger. In another five minutes (51-75, q=2) the rain has significantly decreased, and was gone in another five minutes (76-100, q=3). The same pattern can be seen in the remaining 15 minutes (101-175, q=4-6).

Figure 4.6, on the other hand, shows location detection across three rain categories. Again, location detection was done very effectively. The reliability of the recovered magnitude is also best in light rain and gradually decreases as the rain gets more intense. Even so, the overall rms error for this 70-minute event is only 1.0244.

Another important rain event that the proposed method was able to detect is the presence of localized heavy rain. Figure 4.7 shows an example of a very intense rain event that had an intensity of a violent rain. In this span of 15-minute data, the area was having very light rain, then the torrential rain, and then light rain again. This shows the swiftness of the event. The recovered specific attenuation magnitude is also very close to the actual value, with an error of only 0.1330.

Another set of figures are shown in Figures 4.8 to 4.11, where the rainfall field reconstruction within the 25-point area are illustrated, showing the location and intensity of the specific attenuation at a given time. Different rain intensities were chosen to illustrate the performance of the reconstruction method. The reconstruction was not dependent on the rain rate, since even for very light rains it still performed well. The rms error is also given for each example. How the reconstruction process spreads out the values to neighboring areas is obvious when the simulation results are compared to the actual values, but the error is still negligible. In fact, the overall error for the 13-month data is only 0.2201.

3.1 Reconstruction at Different Climates

The discussion so far involved data from the subtropical region of Okinawa, but it is also interesting to explore how the proposed method will perform in other climates and weather patterns. In this study, two other locations were chosen: Tokyo and Hokkaido in the mid-latitude region. Tokyo is a highly-urbanized city with characteristic small-scale weather patterns, while Hokkaido has a climate similar to temperate countries. The three locations were chosen to show the

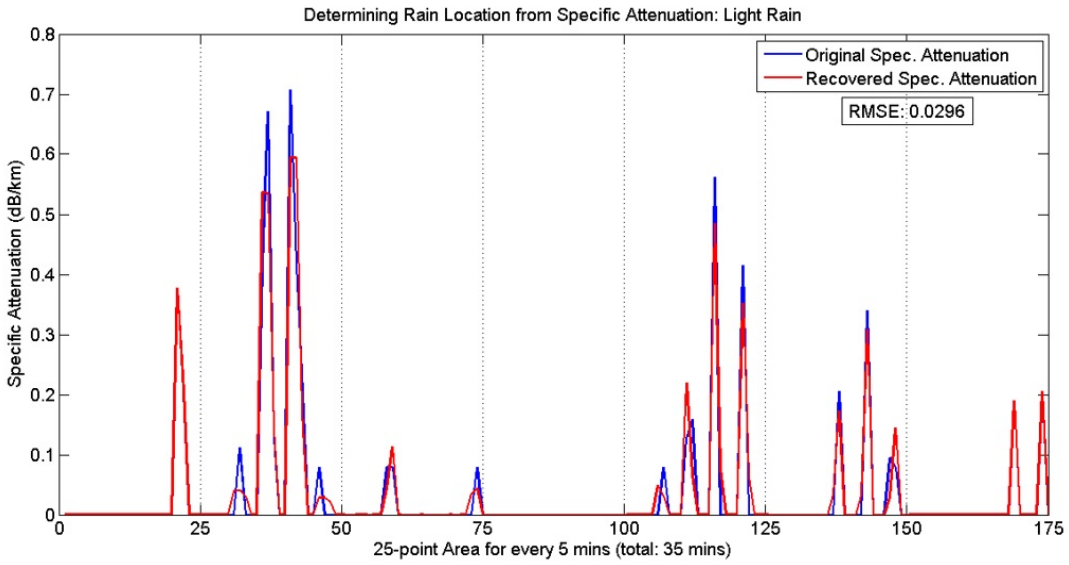

Figure 4.5. Sample rain location detection by the proposed method for light rain.

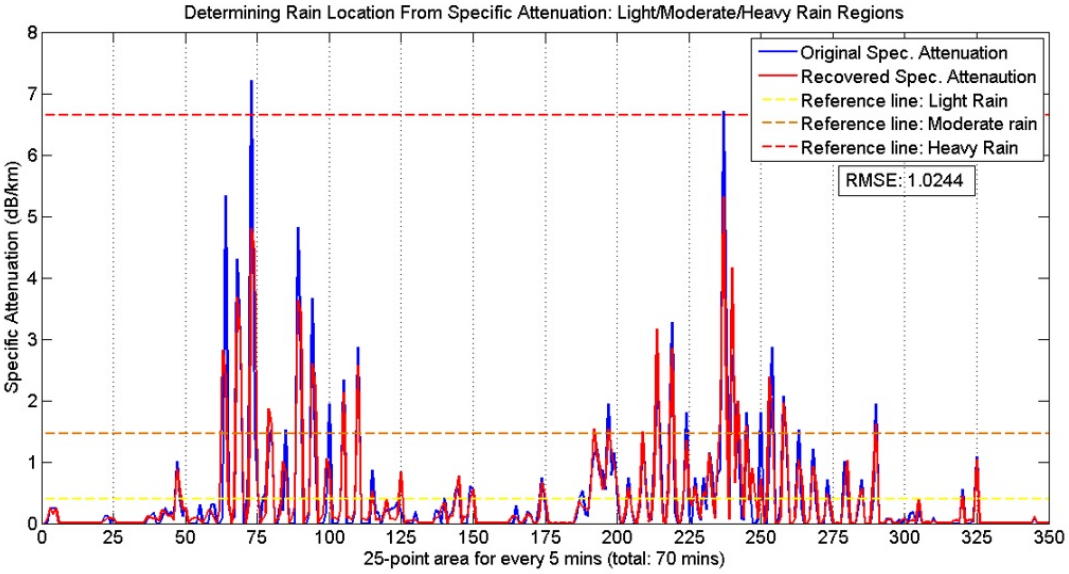

Figure 4.6. Sample rain location detection by the proposed method for light to heavy rain.

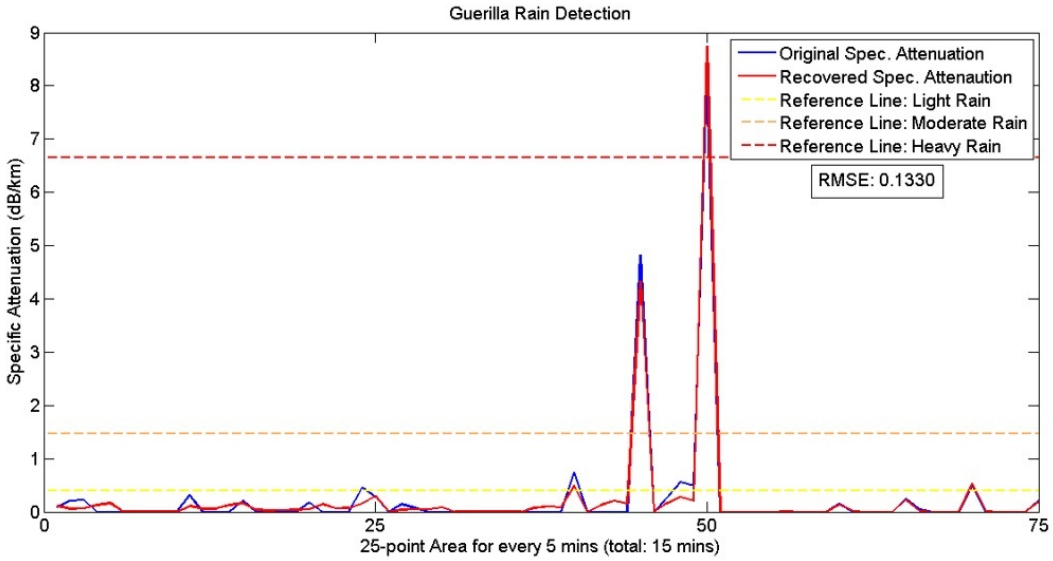

Figure 4.7. Sample rain location detection by the proposed method for guerilla rain.

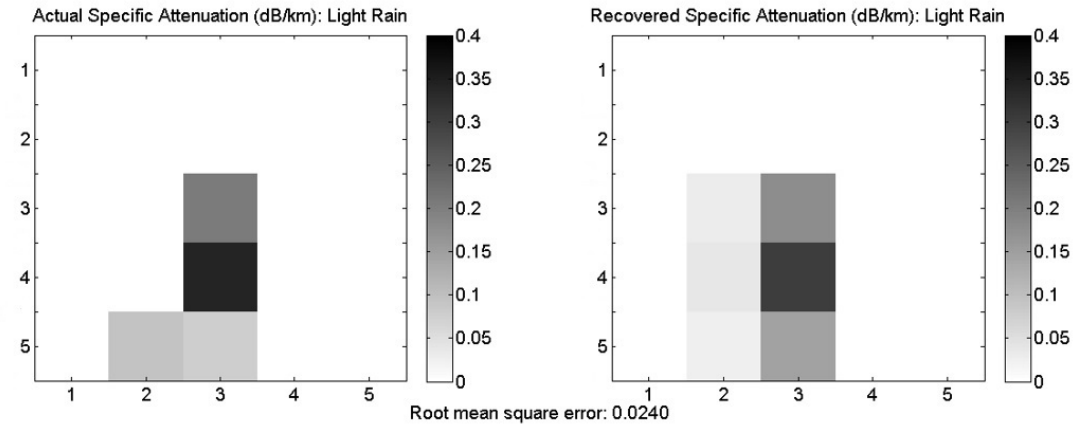

Figure 4.8. Results for location and magnitude detection for light rain.

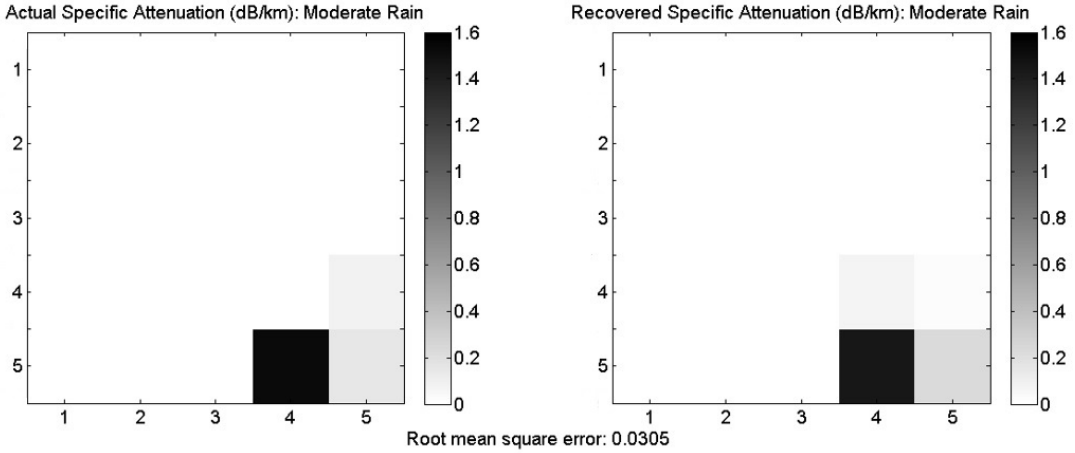

Figure 4.9. Results for location and magnitude detection for moderate rain.

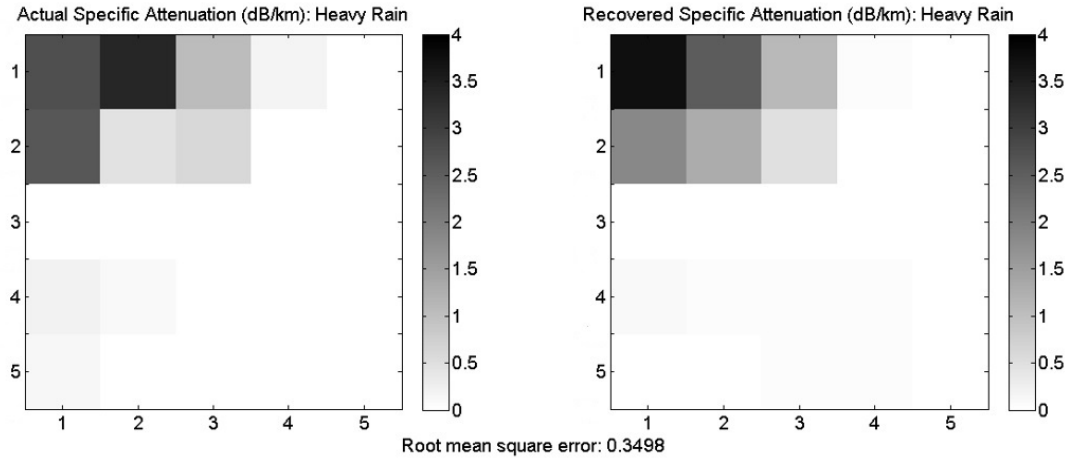

Figure 4.10. Results for location and magnitude detection for heavy rain.

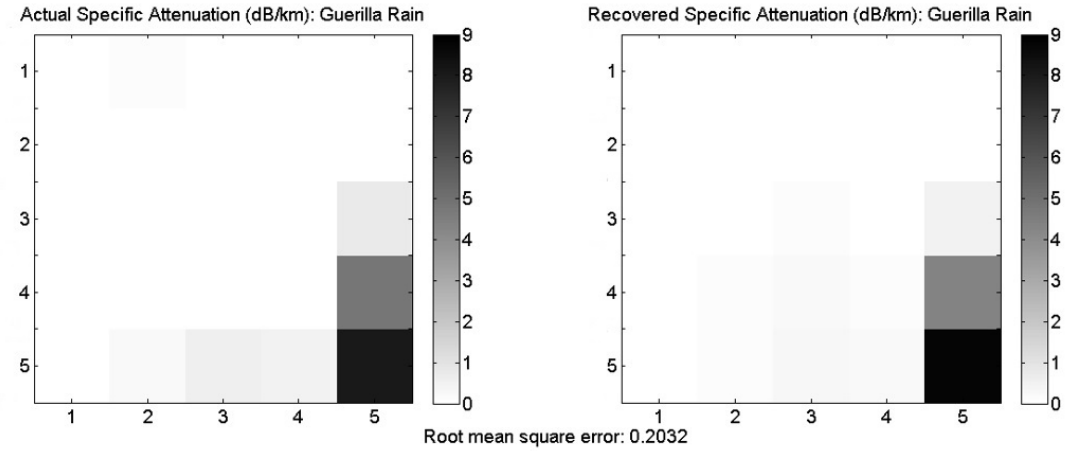

Figure 4.11. Results for location and magnitude detection for guerilla rain.

effects of different possible rain types and durations.

Table 4.2 shows the FPR and FNR for the three locations. It can be seen that the FPR is very much larger than the FNR. As mentioned before, this is because of the spreading of the rain rates to neighboring areas, usually at a lower rain rate. This means that there are many reconstructed data points that have rain values when there should be none. The original FPR is calculated using this No Rain threshold (NR-thresh), which means that the identification of areas with rain depends on whether there is value or not, regardless of the intensity of the rain. However, in reality, these false positives have very small values, in fact very close to 0, that they are practically negligible. This means that improvement in the FPR can be achieved if another threshold is implemented. Table 4.3 shows how the FPR and FNR are improved when the Light Rain threshold (LR-thresh) is implemented. This threshold means that all values that are considered light rain (rain rate of less than 2.5mm/hr and specific attenuation of less than 0.40 dB/km) are considered No Rain areas. With this threshold, the values of FPR and FNR are improved and almost equal to 0.

Also according to Table 4.2, it can be seen that in terms of number, Hokkaido has the most number of rain events, followed by Tokyo, and then by Okinawa. In the same table, the false positive and false negative rates are also given, along with the corresponding rms error. It can be seen that Hokkaido has the worst FPR, meaning in the reconstruction, there were areas that have rain when there

Table 4.2. False Positive and False Negative Rates for Three Different Locations

Location	**% of Rain Events**	**FPR (%)**	**FPR RMSE**	**FNR (%)**	**FNR RMSE**
Hokkaido	13.4	10.3	0.05	7.34×10^{-3}	0.09
Tokyo	11.26	8.7	0.08	6.54×10^{-3}	0.14
Okinawa	11.09	9.6	0.12	1.2×10^{-2}	0.13

Table 4.3. False Positive and False Negative Rates for Three Different Locations, with Threshold

Location	**FPR (NR-thresh)**	**FPR (LR-thresh)**	**FNR (NR-thresh)**	**FNR (LR-thresh)**
Hokkaido	10.3	2.46×10^{-4}	7.34×10^{-3}	3.11×10^{-6}
Tokyo	8.7	7.78×10^{-5}	6.54×10^{-3}	0
Okinawa	9.6	1.26×10^{-3}	1.2×10^{-2}	0

shouldn't be. However, in Table 4.3 it can be seen that more than 90% of the data for Hokkaido has very little or no rain at all and the important rain rates are actually less than 1% of the data. This means that most of the recovered rain rates for the Hokkaido data are small enough to be considered as negligible. Therefore, high FPR is acceptable when we know that the recovered rain rates are negligible. The same can be said for Tokyo and Okinawa, where the majority of the data are in the Light Rain and No Rain categories. The FNR in all three locations are very small, indicating a good detection rate for the proposed method. The rms error values in Table 4.2 were calculated using the reconstruction values and regardless of the rain rate category. Because of this, large rms errors in the heavy to violent rain categories affect the overall rms error. The FNR error for Tokyo shows this. The FNR for Tokyo is between that of Hokkaido and Okinawa but its FNR error is slightly higher than that of Okinawa. This does not necessarily mean that the detection done in Tokyo is less accurate, just that the absolute values of the data used produced an error that is more or less similar to that of Okinawa. The errors per category shown in Table 4.3 indicate that the error values for Tokyo are between Hokkaido and Okinawa.

The evaluation of recovered values based on rain rate is shown in Table 4.4.

Even though Hokkaido has the most number of rain events, it has the least number of destructive rain rates (Heavy and Violent Rain categories). In contrast, Okinawa has the least number of rain events but it has the most number of destructive rain rates. This is to be expected since Okinawa is in the subtropical region that experiences more typhoons throughout the year. In terms of error in recovering the values, it seems that the higher number of extreme rain events, the error is also higher. Tokyo is geographically between Hokkaido and Okinawa, and results for Tokyo are also between the results of the other two locations.

One interesting thing to note for Tokyo is that the percentage of light rain is relatively higher than those for the other two locations. Although it doesn't have as much destructive rain events as Okinawa, it does have a lot of light rain (more than 50% of the whole data). Although the percentage is large, this rain rate intensity does not pose any significant threat in terms of landslides and flash floods. The weather patterns in a highly urbanized city like Tokyo is important to study because meteorologists are now seeing patterns that are noticeable in urban cities but not in rural areas in the same latitude.

In all three locations, the percentage of rains in the heavy and violent rain rate categories is less than 5% of the data, and the error in recovery is also not that big. A more significant error is in the violent rain category (more than 1 dBm). However, in practice the link may have possibly gone down already at these rain rates. This means that it would be hard to determine the exact amount of link attenuation, and what is known for sure is that the rain rate is very high already. In this case, the error in attenuation recovery is not so significant any more, but what is now more important is classifying the rain as violent and that it can possibly trigger disasters like flash floods and landslides.

3.2 Discussion and Conclusion for Fully-covered Area Configurations

Simulation results show that given a 10-link microwave mesh network in a 25 square kilometer area, the rain location and corresponding specific attenuation values can be effectively determined, with errors that are almost practically negligible. If the number of links crossing a single area is increased, the accuracy of

Table 4.4. Evaluation of Recovered Values Based on Rain Rate

Rain Category	**Hokkaido Data Pts: 381, 450**	**Hokkaido RMSE**	**Tokyo Data Pts: 321, 025**	**Tokyo RMSE**	**Okinawa Data Pts: 316, 125**	**Okinawa RMSE**
No Rain	47.09%	0.0377	28.94%	0.0520	46.97%	0.0561
Light	44.56%	0.0487	53.81%	0.0564	33.46%	0.1099
Moderate	7.96%	0.1402	15.07%	0.1755	15.75%	0.2701
Heavy	0.38%	0.5143	2.03%	0.6297	3.65%	0.7724
Violent	4.98×10^{-3}%	1.3318	0.15%	1.7837	0.17%	2.3699

detection and reconstruction for that area also increases. The proposed method proved effective for different rain intensities (light, moderate, heavy, and violent rains). More importantly, it was able to detect the presence of localized heavy rain, with the recovered value very close to the actual value. This can help in mitigating the effects of rain-related disasters like landslides and flash floods.

The proposed method was also applied to locations with different climates and weather patterns. The results show that the method can still reconstruct the rain fields well, and the errors are negligible for practical purposes. These errors are so small and usually not noticed in real time monitoring of microwave links.

The rain field reconstruction was done using a compressed sensing-based algorithm and without using any conventional weather sensing equipment. This shows the advantage of using the proposed method in areas with not much weather radars but with many microwave communication links deployed, like the tropical countries. The scale and temporal resolution of the microwave mesh networks also make it ideal for detecting localized heavy rains that are common in tropical countries. These torrential rains are the usual cause of river swelling that leads to flash floods, and by detecting the presence of these rains, a disaster might be avoided.

4 Network Configurations for Partially-covered 25-point Area

In the network configurations for partially-covered 25-point area, the number of links had been reduced to more realistic numbers in a deployment. The fully-covered 10-link configuration in Fig. 4.2 was used first, then the links were reduced one by one until only one link was used. The same 25-points were reconstructed using the decreasing number of links, and since less areas are covered, the error in reconstruction became bigger.

Figure 4.12 shows the RMSE when link number is decreased from ten to one. This simulation includes all types of rain intensities, from the lightest to the heaviest rainfall. The RMSE is computed by comparing the reconstructed 25-point values with the original 25-point values, therefore it is an evaluation of the rainfall reconstruction even for cases with limited observation data. From L=10 until L=5, all the 25-point areas are covered by at least one microwave link, which means that the whole 25-point area can be reconstructed with non-zero values by the compressed sensing method. The error difference compared to the fully-covered 10-link configuration is not very big. In fact, the RMSE for L=10 and L=9 are almost the same, indicating that a 9-link configuration will achieve almost the same result as a 10-link configuration However, from L=4 to L=1, the links can only partly cover the 25-point area, which means that the places with no links crossing over it will be reconstructed as zero. This made the difference between the original value and the reconstructed values much bigger.

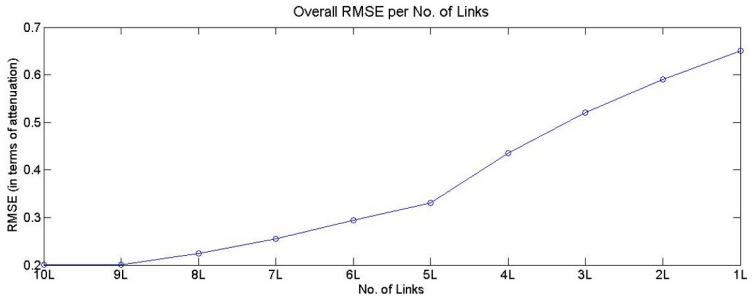

Figure 4.12. Reconstruction error for configurations with decreasing number of links.

Two configurations that only partially cover the 25-point area are considered in this section: 2-link and 3-link configurations. These are shown in Fig. 4.13 and 4.14.

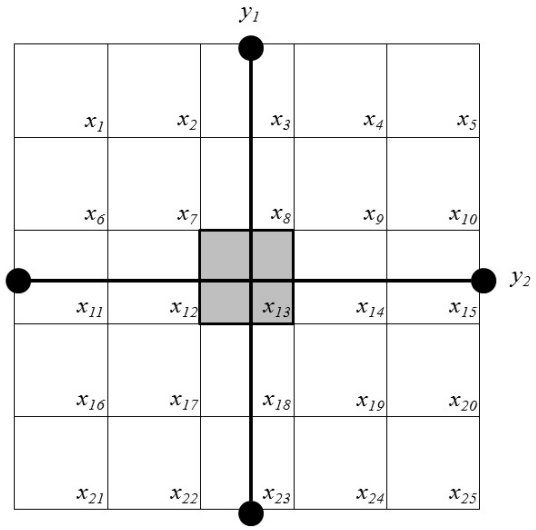

Figure 4.13. Microwave mesh network with two links.

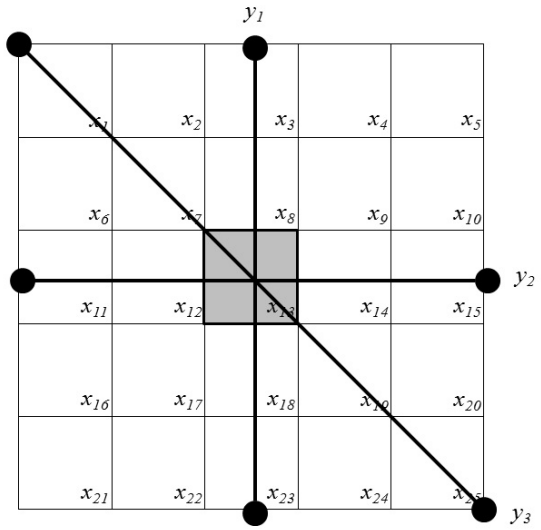

Figure 4.14. Microwave mesh network with three links.

This time again, the values of x_1 to x_{25} where first calculated using Eq. (2.1) and the link attenuation is calculated from Eq. (4.1). For the 2-link and 3-link

configurations, Φ_2 and Φ_3 are given by:

$$\Phi_2 = \begin{bmatrix} 0 & 0 & 1 & 0 & 0 & 0 & 0 & 1 & 0 & 0 & 0 & 0 & 1 & 0 & 0 & 0 & 0 & 1 & 0 & 0 & 0 & 0 & 1 & 0 & 0 \\ 0 & 0 & 0 & 0 & 0 & 0 & 0 & 0 & 0 & 0 & 1 & 1 & 1 & 1 & 1 & 0 & 0 & 0 & 0 & 0 & 0 & 0 & 0 & 0 & 0 \end{bmatrix} \quad (4.6)$$

$$\Phi_3 = \begin{bmatrix} 0 & 0 & 1 & 0 & 0 & 0 & 0 & 1 & 0 & 0 & 0 & 0 & 1 & 0 & 0 & 0 & 0 & 1 & 0 & 0 & 0 & 0 & 1 & 0 & 0 \\ 0 & 0 & 0 & 0 & 0 & 0 & 0 & 0 & 0 & 0 & 1 & 1 & 1 & 1 & 1 & 0 & 0 & 0 & 0 & 0 & 0 & 0 & 0 & 0 & 0 \\ 1 & 0 & 0 & 0 & 0 & 0 & 1 & 0 & 0 & 0 & 0 & 0 & 1 & 0 & 0 & 0 & 0 & 0 & 1 & 0 & 0 & 0 & 0 & 0 & 1 \end{bmatrix}. \quad (4.7)$$

The link attenuation values were then used in the compressed sensing-based reconstruction of the specific attenuation. The same set of lower and upper bounds on x were set to 0 and 25.

The 2-link and 3-link reconstruction results were compared with the 10-link results. There are only 9 areas that are common in all three configurations: x_3, x_8, x_{11}, x_{12}, x_{13}, x_{14}, x_{15}, x_{18}, and x_{23}. The 2-link configuration covers all 9 areas, while the 3-link covers an additional 4 more areas. Because of this, it can be seen from Table 4.5 that there is a slight improvement in the overall RMSE from 2-link to 3-link configuration. The 10-link configuration has the best RMSE because it covered all 25 areas with two links each.

Figure 4.15 shows the RMSE for the 9 common points. It is easier to see from these figures that the improvement between 2-link and 3-link configurations is not very significant. Also, the point of crossing, x_{13}, has a significantly higher RMSE than the other points. However, the FPR and FNR comparisons as shown in Fig. 4.16 and Fig. 4.17 show that x_{13} has the best results. The high RMSE of x_{13} may be caused by the absolute values of the attenuation, but an analysis per rain rate category shows that the violent and heavy rains are still detected. Moreover, it can be seen from Fig. 4.16 that x_{13} is the same for the 2-link and 10-link configurations and slightly better for the 3-link configuration. This is because for the first two cases, there are exactly two microwave links passing through x_{13}, as compared to other points that have only one or no link. Figure 4.17 also shows that as long as there is more than one link passing an area, the FNR practically becomes zero.

The results presented so far are for No Rain threshold. The results for FPR and FNR rates when the Light Rain threshold is implemented is shown in Table

Table 4.5. Overall RMSE for the Three Configurations

	2-Link	**3-Link**	**10-Link**
NR-th	0.7598	0.7207	0.2008
LR-th	0.7647	0.7304	0.4522

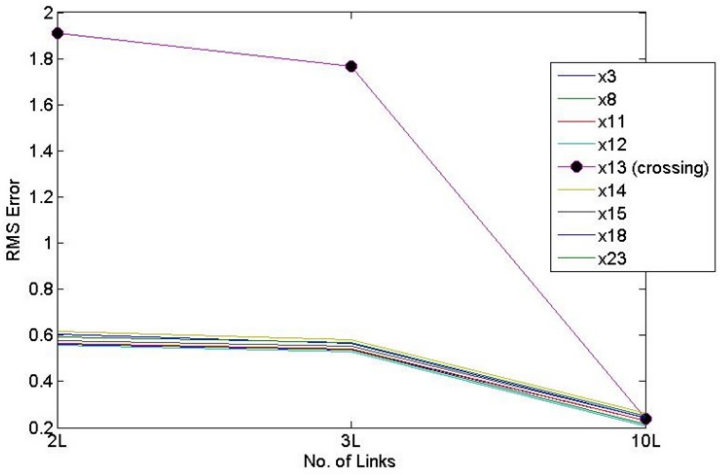

	x3	x8	x11	x12	x13	x14	x15	x18	x23
2L	0.561	0.5639	0.5662	0.559	1.9094	0.619	0.5774	0.6051	0.595
3L	0.5374	0.5376	0.5409	0.5284	1.7665	0.5817	0.555	0.5657	0.5688
10L	0.2311	0.2121	0.2309	0.2068	0.2382	0.2599	0.2431	0.2426	0.2483

Figure 4.15. RMSE per point for the three configurations.

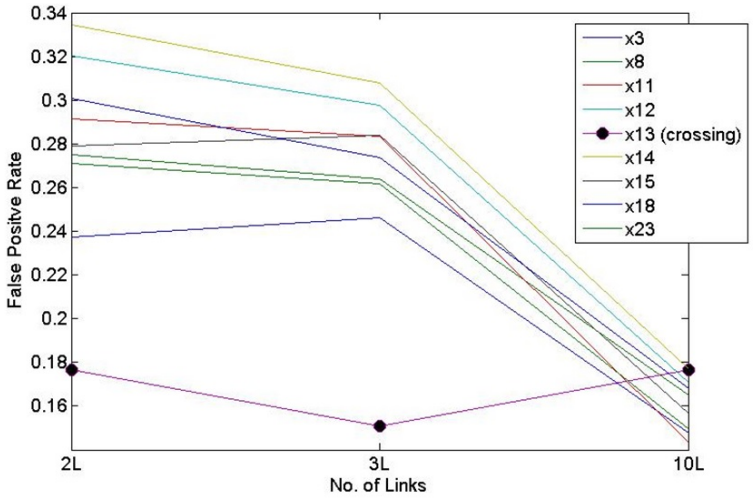

	x3	x8	x11	x12	x13	x14	x15	x18	x23
2L	0.2372	0.2749	0.2914	0.3203	0.1767	0.3345	0.2789	0.3007	0.2712
3L	0.246	0.2639	0.2835	0.2978	0.1507	0.308	0.2838	0.2737	0.2618
10L	0.1479	0.165	0.1433	0.171	0.1767	0.177	0.1568	0.1683	0.1496

Figure 4.16. False positive rate, NR-thresh.

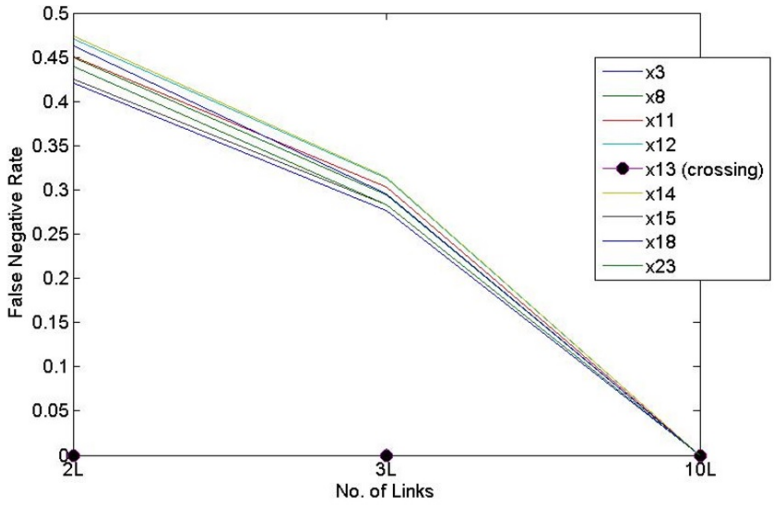

	x3	x8	x11	x12	x13	x14	x15	x18	x23
2L	0.4205	0.4501	0.4508	0.4705	0	0.4747	0.4251	0.4634	0.4393
3L	0.2765	0.2949	0.303	0.3134	0	0.3144	0.2835	0.296	0.2834
10L	0	0	0	0	0	0	0	0	0

Figure 4.17. False negative rate, NR-thresh.

Table 4.6. FPR Improvement Due to Thresholding, L=2,3,10

	FPR (NR-th)			**FPR (LR-th)**		
	2L	3L	10L	2L	3L	10L
x_3	0.2372	0.246	0.1479	0.2026	0.1937	5.22×10^{-3}
x_8	0.2749	0.2639	0.165	0.1947	0.1699	4.77×10^{-3}
x_{11}	0.2914	0.2835	0.1433	0.3122	0.2982	3.91×10^{-3}
x_{12}	0.3203	0.2978	0.171	0.3249	0.2943	3.03×10^{-3}
x_{13}	0.1767	0.1507	0.1767	0.6093	0.5959	3.95×10^{-3}
x_{14}	0.3345	0.308	0.177	0.3122	0.2749	5.15×10^{-3}
x_{15}	0.2789	0.2838	0.1568	0.2487	0.2456	3.50×10^{-3}
x_{18}	0.3007	0.2737	0.1683	0.2579	0.2233	2.15×10^{-3}
x_{23}	0.2712	0.2618	0.1496	0.2737	0.2391	3.44×10^{-3}

4.6 and 4.7. As can be seen in the tables, applying the LR threshold to the 2-link and 3-link configurations did not improve the FPR and FNR rate. The FPR after applying the threshold was either improved or worsened but was more or less the same value. This is because there is not much spreading of rain to neighboring areas as compared to when all 25-points area being recovered (as in the 10-link case). As for the FNR, it got worse after applying the LR threshold. This is because in the reconstructed results, the areas with no links over it are recovered with a value of 0, which is most likely not true if compared to the real data. Therefore, when the LR-threshold is implemented, it further made more areas to have a value of 0, making the FNR worse. Table 4.6 also shows clearly that for areas defined by at least two microwave links, the possibility of a false negative reconstruction is 0. This means that the FNR can be easily improved by adding another link in the area.

4.1 Conclusion for Partially-covered Area Configurations

The network configurations that partially cover the 25-point area were simulated to create more realistic mesh networks over a 5 km by 5 km area. A per-area analysis was made for the FPR, FNR, and RMSE for 2-, 3-, and 10-link configurations. The area with the crossing links (x_{13}) has the best results in the

Table 4.7. FNR Improvement Due to Thresholding, L=2,3,10

	FNR (NR-th)			**FNR (LR-th)**		
	2L	3L	10L	2L	3L	10L
x_3	0.4205	0.2765	0	0.8657	0.8191	0
x_8	0.4501	0.2949	0	0.8642	0.8137	0
x_{11}	0.4508	0.303	0	0.8792	0.8395	0
x_{12}	0.4705	0.3134	0	0.8826	0.8402	0
x_{13}	0	0	0	0	0	0
x_{14}	0.4747	0.3144	0	0.8799	0.8352	0
x_{15}	0.4251	0.2835	0	0.8661	0.8249	0
x_{18}	0.4634	0.296	0	0.8756	0.8267	0
x_{23}	0.4393	0.2834	0	0.8809	0.8339	0

reconstruction. It was also found out that there's not much difference in the results between the 2-link and 3-link configurations. The FPR and FNR results are also not improved with the application of LR threshold. The FNR result can be improved by putting 2 links in the same area.

5 Conclusion

Rainfall attenuation of microwave mesh networks can be used as input to a rain sensing system, without the additional cost of other weather sensors and high-end equipment. This chapter has demonstrated that with the use of compressed sensing algorithm, the specific attenuation, and subsequently the rain rate, of areas where a microwave link passes through can be derived from the link attenuations of the mesh network. The total number of links in a configuration and the number of crossing links affect the accuracy of detection: more areas covered by multiple links will give a more accurate rainfall field reconstruction and additional links crossing a single area improves the FNR and FPR. The simulation results have shown that the method can detect even the sporadic heavy rains that are difficult to observe. The proposed method works for all rain intensities as shown in the results, but it works better for the higher rain rates that happen

in smaller areas. This is because the compressed sensing algorithm requires that the data to be reconstructed is sparse or at least most of the values are zero or can be regarded as zero. The locations of the high rain rates were also determined accurately as shown by the false positive and false negative rates. The proposed system can complement existing weather sensing systems and has the potential to act as a standalone rainfall sensor in areas where traditional weather sensors are not available. Urban areas that are at risk with the localized heavy rains will benefit from the proposed method because of the high number of microwave links deployed over it.

Chapter 5

Conclusion

In recent years, the frequency of occurrence and intensity of typhoons and tropical storms have been increasing, which may be attributed as effects of climate change. Even typhoon paths are changing, as more and more places that barely experienced storms before are now being damaged by strong typhoons, due mainly to the lack of experience and preparedness with these kinds of weather phenomena. Aside from these, recently weather anomalies have been observed, in particular the localized intense heavy rains so called "guerilla rain" in Japan. In general, guerilla rains are just like tropical storms that form with the right conditions of temperature, humidity, and pressure, and are characterized as sporadic local heavy rainstorms that are not associated with other mesoscale weather systems. However, when these storms have intense rain rates over a small area, they may cause disasters like flash floods and landslides. In Japan's case, attention was drawn to guerilla rain when 3 incidents between 2008-2009 in Tokyo, Kobe, and Okinawa caused the death of several people due to the rapid increase of river and sewage water levels. Since then, more focus is given to this particular type of rainfall and meteorologists and disaster scientist alike are studying how it forms, the duration of an event, and the possible disaster risks.

Sporadic heavy rains are also more commonly observed in the tropical region, where the lack of weather observation instruments is a significant problem. Observing sporadic heavy rain is hard because of the small area that it occupies, and forecasting its formation and movement is even harder because it can form and dissipate in as fast as 30 minutes. Conventional weather sensors include

weather radars and satellites, but the coverage area is too wide and might not give an accurate ground level rain estimate. On the other hand, local weather stations capable of measuring precipitation, temperature, wind speed and direction, among others, can give a better ground level rain estimate but are usually deployed several kilometers away from each other.

To detect sporadic heavy rains at the appropriate scale, this research uses the attenuation of microwave mesh networks. These networks have effective covered areas that fit the size of the rain clouds. Moreover, they are already deployed as commercial links, minimizing the added cost for turning the system into a weather sensor. Microwave links are also greatly attenuated by rainfall, but the same rain attenuation can be used to detect and reconstruct the rainfall field without using other weather sensors. Prediction methods and design models like ITU-R P.530 and the Global Crane Model have been widely used to design microwave networks that can withstand rain attenuation and still keep the same quality of service. Also in this study, the rainfall rate in an area is derived from the microwave link attenuation using a new technique called compressed sensing. This technique can reconstruct a signal or an image using a limited number of measurements and certain conditions.

In the first part of the study, the effect of rain attenuation on microwave mesh networks was studied in the context of route diversity. Route diversity is a technique to lessen the effect of rain attenuation on the delivery of information of mesh networks. Chapter 3 looked into the links' orientation and separation by 90° and 180° angles as ways to implement the route diversity. The convergent path elements and simple four-node square configurations were simulated using real rainfall data to see the difference for links oriented in different directions. The results show that the diversity gain and diversity improvement are highest for the 180° link configurations. This is because these configurations have the biggest angle of separation and therefore the lowest probability for both links to experience the same rain event at the same time. From the analysis of the four-node square configuration, there was a significant diversity gain even for a two-hop relay, with preference on the path that includes a south-oriented link.

The next part of the study is about reconstructing the location and intensity of the rainfall field from the attenuation of the mesh network. Rainfall attenua-

tion of microwave mesh networks can be used as input to a rain sensing system, without the additional cost of other weather sensors and high-end equipment. This research has demonstrated that with the use of a compressed sensing-based algorithm, the specific attenuation, and subsequently the rain rate, of areas where a microwave link passes through can be derived from the link attenuations of the mesh network. The total number of links in a configuration and the number of crossing links affect the accuracy of detection: more areas covered by multiple links will give a more accurate rainfall field reconstruction and additional links crossing a single area improves the FNR and FPR. The simulation results have shown that the method can detect even the sporadic heavy rains that are difficult to observe. The proposed system can complement existing weather sensing systems and has the potential to act as a standalone rainfall sensor in areas where traditional weather sensors are not available.

Acknowledgements

This research became possible because of the following institutions: the Japanese Government (Monbukagakusho: MEXT) Scholarship, the Network Systems Laboratory of Nara Institute of Science and Technology, and the Department of Electronics, Communications, and Computer Engineering of the Ateneo de Manila University.

Thanks to Prof. Minoru Okada for being a great supervisor who is always willing to lend his ideas, comments, and invaluable support during the period of this research.

Thanks to Assoc. Prof. Takeshi Higashino and former Assoc. Prof. Takao Hara for all the valuable comments and help you have given me during my stay in the laboratory.

Thanks to my thesis co-supervisors Prof. Hiroyuki Seki, Prof. Keiichi Yasumoto, and Assoc. Prof. Takeshi Higashino for their comments and support to improve this work.

Thanks to everyone who were part of the Communications Laboratory and Network Systems Laboratory for all the help, support, and fun experiences that you shared with me. I hope we can see each other again in the future.

Thanks to everyone in Ateneo de Manila University, especially to the ECCE Dept., Dr. Nathaniel Joseph Libatique, and Dr. Gregory Tangonan for always being there to help and support this project. Thank you for the hospitality whenever we need to go to Manila and for the great discussions that helped shape this research.

Thanks to everyone who have been part of this rain research — then, now, and in the future. May we always remember the significance of what we are doing, especially when it seems to be a never-ending work.

Thanks to the Japanese and international students who became my friends here in Japan. You guys definitely made my whole Japan experience very fun and exciting. Special thanks go to the Filipino community here in NAIST for being a second family to me. More special thanks go to Erlyn Manguilimotan for the friendship and all the support in the last 4 years. I hope I can see you all again in the future, even as we go back to our home countries.

Thanks to my family and friends for all the love, trust, help, and support you have given me all these years. Thanks for putting up with me and my obsession with rain.

Thanks for all the help, encouragement, and love you gave me as I went through these past stressful months. I wouldn't have made it this far without going crazy and wouldn't have finished this dissertation without you. I'm forever grateful.

Thank You Lord for all the wisdom and the strength and the hope You have given me.

Thank you. Thank you. Thank you.

Publications

Journal

1. Gemalyn Dacillo Abrajano and Minoru Okada, "Rainfall Field Reconstruction Using Rain Attenuation of Microwave Mesh Networks," in *ECTI Transactions on Computer and Information Technology*, vol. 7, no. 2, pp. 118-126, November 2013.

International Conferences

1. Gemalyn Dacillo Abrajano and Minoru Okada, "Route Diversity for Microwave Mesh Network Based on Angular Separation and Link Orientation," in *2011 Asia-Pacific Microwave Conference (APMC) Proceedings*, pp. 670-673, Melbourne, Australia, December 2011.

2. Gemalyn Dacillo Abrajano and Minoru Okada, "Determining Rain Location Through Microwave Mesh Network Signal Attenuation," in *2012 IEEE Region 10 Conference (Tencon)*, pp. 1-6, Cebu, Philippines, November 2012.

3. Gemalyn Dacillo Abrajano and Minoru Okada, "Compressed Sensing Based Detection of Localized Heavy Rain Using Microwave Network Attenuation," in *2013 7th European Conference on Antennas and Propagation (EuCAP)*, pp. 2383-2386, Gothenburg, Sweden, April 2013.

Domestic Conferences

1. Gemalyn Dacillo Abrajano and Minoru Okada, "Performance Analysis on Route Diversity for Microwave Mesh Network Based on Angular Separation and Link Orientation," in *IEICE Technical Report, Smart Info-Media System Technical Meeting*, vol. 111, no. 457, pp. 139-143, Tokyo, Japan, March 2012.

2. Gemalyn Dacillo Abrajano, Takeshi Higashino, and Minoru Okada, "Detection of Sporadic Heavy Rain Using Rainfall Attenuation in Microwave Mesh Network," in *IEICE Technical Report, Smart Info-Media System Technical Meeting*, vol. 113, no. 343, pp. 105-110, Tottori, Japan, December 2013.

References

[1] IPCC, 2013: Summary for Policymakers. In: Climate Change 2013: The Physical Science Basis. Contribution of Working Group I to the Fifth Assessment Report of the Intergovernmental Panel on Climate Change [Stocker, T.F., D. Qin, G.-K. Plattner, M. Tignor, S. K. Allen, J. Boschung, A. Nauels, Y. Xia, V. Bex and P.M. Midgley (eds.)]. Cambridge University Press, Cambridge, United Kingdom and New York, NY, USA.

[2] C. Mora, et al., "The Project Timing of Climate Departure from Recent Variability," *Nature*, vol. 502, October 2013, pp. 183-187.

[3] D. Vergano. "Friday's Big Global Warming Report: 5 Takeaways." Internet: http://news.nationalgeographic.com/news/2013/13/130927-ipcc-report-released-climate-change-global-warming-intergovernmental-panel-on-climate-change/, Sept. 27, 2013 [Dec. 11, 2013].

[4] National Research Council. "Abrupt Impacts of Climate Change: Anticipating Surprises." Washington, DC: The National Academies Press, 2013.

[5] J. Timmer. "US National Research Council Wants Abrupt Climate Change Warning System." Internet: http://arstechnica.com/science/2013/12/us-national-research-council-wants-abrupt-climate-change-warning-system/, Dec. 5, 2013 [Dec. 11, 2013].

[6] D. Vergano. "Abrupt Climate Disaster Threat Raises Call for Early Warning System." Internet: http://news.nationalgeographic.com/news/2013/12/131203-abrupt-climate-change-science-early-warning-report/, Dec. 3, 2013 [Dec. 11, 2013].

[7] M. Fischetti. "Was Typhoon Haiyan a Record Storm?" Internet: http://blogs.scientificamerican.com/observations/2013/11/12/was-typhoon-haiyan-a-record-storm/, Nov. 12, 2013 [Dec. 11, 2013].

[8] "In 'Guerilla Rain' Fight, the Key Weapon is Data." *The Yomiuri Shinbun*, 17 July 2010. Retrieved May 15, 2012, http://www.yomiuri.co.jp/dy/editorial/20100718TDY02T02.htm.

[9] Japan Meteorological Agency. Retrieved May 15, 2012. http://www.jma.go.jp/en/amedas_h/map65.html?areaCode=217.

[10] ITU-R P. 530-10. *Propagation Data and Prediction Methods Required for the Design of Terrestrial Line-Of-Sight Systems.*

[11] J. Seybold. "Rain Attenuation of Microwave and Millimeter Wave Signals" in *Introduction to RF Propagation*, Wiley and Sons, Inc., 2005, pp.229-234.

[12] H. Leijnse, R. Uijlenhoet, and J. Stricker. "Rainfall Measurement Using Radio Links from Cellular Communication Networks," *Water Resource Res.*, Vol. 43, No. 3, 2007.

[13] A. Zinevich, P. Alpert, and H. Messer. "Estimation of Rainfall Fields Using Commercial Microwave Communication Networks of Variable Density," *Adv. Water Resource*, 2008.

[14] G. Upton, A. Hold, R. Cummings, A. Rahimi, and J. Goddard. "Microwave Links: The Future of Urban Rainfall Measurement?," *Atmos. Res.*, Vol. 77, No. 14, pp. 300312, 2005.

[15] N. J. C. Libatique, et al. "Design of a Tropical Rain - Disaster Alarm System." *International Instrumentation and Measurement Technology Conference*, May 2009.

[16] H. Messer, A. Zinevich, and P. Alpert, "Environmental Monitoring by Wireless Communication Networks," *Science*, vol. 312, p. 713, 2006.

[17] A. R. Rahimi, A. R. Holt, G. J. G. Upton, and R. J. Cummings. "The Use of Dual-Frequency Microwave Links for Measuring Path-Averaged Rainfall," *J. Geophys. Res.*, 2003, 108(D15), 4467.

[18] A. Berne and R. Uijlenhoet. "Path-Averaged Rainfall Estimation Using Microwave Links: Uncertainty Due to Spatial Rainfall Variability," *Geophysical Research Letters*, Vol. 34, 2007.

[19] R. Nelson. "Rain: How It Affects the Communication Links," via *Satellite Magazine*, May 2000.

[20] ITU-R P. 837-4. *Characteristics of Precipitation for Propagation Modelling.*

[21] G. Hendrantoro, R. J. C. Bultitude, and D. D. Falconer. "Use of Cell-Site Diversity in Millimeter-Wave Fixed Cellular Systems to Combat the Effects of Rain Attenuation," *IEEE Journal on Selected Areas in Communications*, vol. 20, no. 3, pp. 602-614, April 2002.

[22] Z. A. Shamsan, M. I. Abo-zeed, and J. Din. "Rain Fading Mitigation in BWA Using Site Diversity," *2007 Asia-Pacific Conference on Applied Electromagnetics Proceedings*, December 2007.

[23] ITU-R P. 1410-4. *Propagation Data and Prediction Methods for the Design of Terrestrial Broadband Radio Access Systems Operating in a Frequency Range from 3 to 60 GHz.*

[24] E. C. Van der Muelen, "Three-Terminal Communication Channels," *Advances in Applied Probability*, Spring 1971, vol. 3, no. 1, pp. 120-154

[25] ITU-R P. 838-3. *Specific Attnenuation Model for Rain for Use in Prediction Methods.*

[26] C. Matzler, E. Koffi, and A. Berne, "Monitoring Rain Rate with Data from Networks of Microwave Transmission Links," *European Conference on Antennas and Propagation*, Berlin, 2009, pp.907-910.

[27] O. Goldshtein, H. Messer, and A. Zinevich, "Rain Rate Estimation Using Measurements from Commercial Telecommunication Links," *IEEE Trans. Signal Process.*, vol. 57, no.4, pp.1616-1625, Apr. 2009.

[28] D. L. Donoho, "Compressed Sensing," *IEEE Trans. Inf. Theory*, vol. 52, no. 4, pp.1289-1306, Apr. 2006.

[29] E. J. Candes, J. Romberg, and T. Tao, "Robust Uncertainty Principles Exact Signal Reconstruction from Highly Incomplete Information," *IEEE Trans. Inf. Theory*, vol. 52, pp.489-509, Feb. 2006.

[30] E. J. Candes and M. B. Wakin, "An Introduction to Compressive Sampling," *IEEE Signal Processing Mag.*, pp.21-30, Mar. 2008.

[31] M. Davenport, "The Fundamentals of Compressive Sensing," *IEEE Signal Processing Society Online Tutorial Library*, April 12, 2013.

[32] C. Moler, "Magic Reconstruction: Compressed Sensing," Retrieved May 15, 2012. www.mathworks.com.

[33] "Glossary of Meteorology (June 2000): Rain", American Meteorological Society. Retrieved May 15, 2012. http://amsglossary.allenpress.com/glossary/search?id=rain1.

[34] Abrajano and Okada, "Determining Rain Location Through Microwave Mesh Network Signal Attenuation," 2012 IEEE Region 10 Conference, Philippines, November 2012.

[35] R. Olsen, D. Rogers, and D. Hodge. "The aR Relation of Rain Attenuation," *IEEE Trans. Antennas Propag.*, Vol. AP-26, pp. 318328, 1978.